Information in the term structure of yield curve volatility

Anna Cieslak and Pavol Povala*

We study information in the volatility of US Treasuries. We propose a no-arbitrage term structure model with a stochastic covariance of risks in the economy, and estimate it using high-frequency data and options. We identify volatilities of the expected short rate and of the term premium. Volatility of short rate expectations rises ahead of recessions and during stress in financial markets, while term premium volatility increases in the aftermath. Volatile short rate expectations predict economic activity independently of the term spread at horizons up to one year, and are related to measures of monetary policy uncertainty. The term premium volatility comoves with a more general level of economic policy uncertainty. We also study channels through which volatility affects model-based inference about the yield curve.

This version: September, 2013
JEL classification: E43, C51

*Cieslak is at the Northwestern University, Kellogg School of Management. Povala is at the University of London, Birkbeck. Cieslak: a-cieslak@kellogg.northwestern.edu, Department of Finance, Kellogg School of Management, Northwestern University, 2001 Sheridan Road Evanston, IL 60208, phone: +1 847 467 2149. Povala: p.povala@bbk.ac.uk, Birkbeck, University of London, Malet Street, Bloomsbury, London WC1E 7HX, UK, phone: +44 207 631 6486. We thank Torben Andersen, Luca Benzoni, Snehal Banerjee, John Cochrane, Jerome Detemple, Paul Söderlind, Viktor Todorov, Fabio Trojani, Pietro Veronesi, Liuren Wu, Haoxiang Zhu and seminar and conference participants at the NYU Stern, Federal Reserve Bank of New York, Federal Reserve Bank of Chicago, Bank of Canada, Baruch College, University of St. Gallen, WFA, EFA, SoFiE, Institute Luis Bachelier, EC^2, European Winter Finance Summit for their comments.

A vast literature studies and decomposes the information contained in the nominal Treasury yield curve. Perspectives vary from latent factors, reduced-form macro-finance models, through structural settings but most of the time they serve the objective of understanding the Treasury risk premia and short rate expectations. The majority of the recent term structure literature has tackled this and related questions assuming constant volatility. That focus can be justified with tractability and the known difficulties with the joint modeling of the first and second moments of yields. Consequently, relatively little is known about information embedded in the Treasury market volatility.

As the largest and the most liquid debt market in the world, US Treasuries provide investors, central banks and governments worldwide not only with the store of value and liquidity but also serve as the main source of collateral in various transactions. The fluctuations in Treasury yields and in their volatility have impact on a range of asset markets. A rise in interest rate volatility may signal macroeconomic uncertainty, but might also lead to an increase in haircuts for Treasury bonds used as collateral in about half of the repo transactions, and thus diminish the lending capacity in the financial system.[1] These considerations make the understanding of interest rate volatility especially compelling.

In this paper, we ask what we can learn about the term structure and the economy by studying the time-varying second moments of the Treasury yield curve. Relative to the previous literature, our approach is comprised of several new elements: First, to identify the properties of interest rate volatility, we rely on nearly 20 years worth of high-frequency data on transactions in the US Treasury market. The dataset allows us to construct the realized covariance matrix of zero-coupon yields across different maturities. Additionally, we augment the realized co-volatility estimates with information from Treasury derivatives, covering risk-adjusted market expectations of volatility at several points along the yield curve. Second, we propose a no-arbitrage term structure model that is able to accommodate the multivariate dynamics of yield volatilities that we find in the data. In particular, we model the entire stochastic covariance matrix of risks in the economy. This setting imposes a structure on our data through a joint estimation that involves yields, their realized

[1] According to SIFMA quarterly report, in the third quarter of 2010 the outstanding volume of repos and reverse repos among primary dealers in US government securities exceeded $4.62 trillion on average per day (SIFMA, 2010). The argument that increased volatility of Treasuries can lead to diminished lending capacity in the system has gained traction in recent years among practitioners as the outlook for the US economy has become more uncertain and the government debt remains at historically high levels (see e.g. JP Morgan, 2011).

covariance matrix and implied volatilities. With its guidance, we uncover and interpret a factor structure in interest rate volatility.

Our first set of results focuses on the economic interpretation of the volatility dynamics. Interest rate volatility moves around because of either volatile short rate expectations or volatile risk premia. To the extent that short rate expectations reflect market expectations about the path of monetary policy, understanding fluctuations of interest rate volatility over the business cycle is informative about the amount of uncertainty surrounding that path.

The model decomposes information in realized covariances and implied volatilities into three components: two volatility states, which we term as the short- and long-end volatility, and a covariance state. The short-end volatility is the key element driving the variance of short rate expectations; the long-end volatility instead determines the variance of the term premia. The covariance state generates the conditional comovement between shocks to short rate expectations and premia. We study the empirical properties of these factors at different maturities and over time. Perhaps not surprisingly, the volatility of the two-year bond is mostly determined by the expectations part, while that of the ten-year bond by the term premium part. Volatile short rate expectation rather than term premia produce the well-known hump in the unconditional term structure of yield volatilities at maturity of about three years. In terms of time series properties, we find that the short rate expectations component of volatility is shorter lived and less persistent, with a half-life of about half that of the term premium volatility.

Consistent with its link to short rate expectations, short-end volatility rises in anticipation of recessions and during period of distress in asset markets: In our sample period, its highest levels coincide with monetary policy easings. In those episodes, the long-end volatility remains contained, suggesting that risk premia are initially relatively stable; their most pronounced fluctuations, instead, take place at the exit from a recession. A case in point is the financial crisis of 2007/09. Our estimates suggest that the volatility of short rate expectations rises dramatically already in the early summer of 2007 when the symptoms of the subprime crisis become apparent, and it starts to decline as the Fed hits the zero-lower bound in December 2008. At the same time, the risk premium volatility reaches record lows just ahead of the Lehman collapse and only begins increase in the first half of 2009, remaining elevated though the end of our sample in 2010.

By modeling the stochastic covariance of risks in the yield curve, we are able to study the comovement between short rate expectations and the term premia. In this way, we cast new light on the tradeoffs faced by the Fed. During the last two decades, the model implies that the conditional correlation between the term premium and short rate expectations is on average slightly positive (average correlation is below 0.2) but highly time varying. Interestingly, the correlation increases during the long easing episode in 2000/03, and declines afterwards. The model interprets the Greenspan's conundrum period as a gradual decline of the correlation between short rate expectations and the term premium.

As part of our analysis, we document how volatility dynamics determined by the model can be linked to macro-finance observables. We verify our interpretation of volatility states using common uncertainty measures that are independent of asset prices. Specifically, we find that the short-end (short rate expectations) volatility comoves with the level of uncertainty about the monetary policy visible in professional survey forecasts, whereas the long-end (term premium) volatility is correlated with the amount of the economic policy uncertainty. The latter is measured with the index of Baker, Bloom, and Davis (2013), and captures mostly the uncertainty about taxes, spending and regulatory policies.

Our results suggest that interest rate volatility contains additional information about the economy that cannot be read from the standard yield curve factors alone. It is known that the slope of the term structure predicts economic activity at horizons between one and two years ahead. We show that, over our sample period, the short-end volatility forecasts growth at horizons up to one year, and its forecasting power is separate from that of the slope. This is in line with short-rate expectations becoming increasingly volatile ahead of bad times.

We also establish how interest rate volatility interacts with liquidity in asset markets. There exists an interesting lead-lag relationship between yield curve volatility and market-wide liquidity proxies as constructed by Pastor and Stambaugh (2003) for the equities, and Hu, Pan, and Wang (2012) for Treasury bonds. We find that deteriorating liquidity conditions forecast an increase in the term premium (long-end) volatility with a lag up to above a year. However, we fail to find a similarly strong link with the volatility of short rate expectations. Rather, similar to its ability to predict slowdown in economic activity, an increased short-end volatility preempts worsening liquidity several quarters ahead.

Our second set of results concerns the channels through which volatility influences the first moments of interest rates. First, we show that volatility states have a close to imperceptible

effect on the cross sections of yields. In that we do not impose any a priori restrictions and, at the same time, ask the model to match the volatility in the data, this result extends the evidence in the literature on unspanned or hidden factors. For instance, consistent with the notion of hidden factors, we find that the short-end volatility has less than one basis point cross-sectional effect on the term structure, but it contains predictive information about the future macro environment. Second, while we allow volatility risk to be priced, and to impact bond risk premia, we find also this channel not to be quantitatively important. The Treasury term premium can be associated almost entirely with the priced yield curve shocks rather than volatility shocks. Likewise, we do not find evidence that volatility generates predictable variation in bond excess returns in the last two decades. Nevertheless, the model generates realistic dynamics of bond variance risk premium implying that on average investors pay a premium to hedge interest rate volatility risk. The variance risk premium is the highest at the three-year maturity and declines afterwards.

Related literature

Our paper is related to the literature on realized volatility, term structure models with stochastic volatility, and the research into the role of US Treasury bonds in liquidity provision.

Recent advances in high-frequency econometrics have encouraged a model-free look into the statistical properties of bond volatility. Andersen and Benzoni (2010) test empirically the volatility implications of affine term structure models (ATSMs) using realized volatility over the 1991–2000 period. In line with the early evidence in Collin-Dufresne and Goldstein (2002), they find that systematic volatility factors are largely independent from the cross section of yields, and call for extensions of the popular models in the volatility dimension.[2]

In the latent factor domain, several recent papers document that benchmark models with stochastic volatility face difficulties in explaining variation in yield volatility, and those difficulties become increasingly severe at the long end of the yield curve. Collin-Dufresne, Goldstein, and Jones (2009, CDGJ) report that over the 1988–2005 sample, the variance series generated by a standard three-factor model, $A_1(3)$, are essentially unrelated to the model-free conditional volatility measures. Using the same model, Jacobs and Karoui (2009) find a correlation between model-implied and EGARCH volatility reaching up to

[2]Several other papers document a weak relation between the bond volatility, realized as well as derivative-based, and the spot yield curve factors, e.g. Heidari and Wu (2003), and Li and Zhao (2006).

75% over the 1970–2003 period. However, in the more recent sample (1991–2003) this correlation breaks down and becomes negative at the long end of the curve. In a study of Japanese yields at the zero lower bound, Kim and Singleton (2012) arrive at a similar conclusion based on several models. These authors suggest that additional volatility factors may be needed to explain the volatility at the long maturity range. We contribute to this discussion by proposing a new term structure model that accommodates the multivariate nature of yield volatilities, and support its estimation with the information from the realized covariance matrix of yields and implied volatilities. We find that these two elements of our approach alleviate the problems with generating realistic volatility dynamics documented in the literature, allowing us to focus on their economic interpretation.

Andersen, Bollerslev, Diebold, and Vega (2007) and Jones, Lamont, and Lumsdaine (1998) show that relative to other liquid asset markets, bond prices tend to provide a clear and pronounced reaction to economic news. These studies suggest that a rich economic content is present in bond volatilities. The model-based decomposition of the yield volatility allows us to study how its distinct components related to short rate expectations and term premia interact with measures of economic and financial conditions.

Several studies introduce stochastic volatility into macro-finance term structure models.[3] Adrian and Wu (2009) and Campbell, Sunderam, and Viceira (2013) highlight the importance of a stochastic covariance between the real pricing kernel and expected inflation in determining excess bond returns. These models attach economic labels to different yield volatility components. However, understanding the dynamics and the determinants of the yield volatility per se is not in their direct focus. Our paper is the first to study the properties of volatilities decomposing them into risk premium and short rate expectations components. We show that such a decomposition yields new insights about risks in Treasury bonds that cannot be in inferred from yield levels alone.

Given the role that US Treasuries play in the financial system, it is important to understand how volatility of bonds relates to the fluctuations in demand for liquidity and collateral. A growing literature focuses on extracting information about liquidity from the cross section of bonds with different age (e.g. Vayanos and Weil, 2008; Fontaine and Garcia, 2012). Recently, Hu, Pan, and Wang (2012) compose a noise illiquidity measure as an average yield pricing error of Treasury bonds. Using our model-based decomposition of yield volatility,

[3]Examples of such models are Campbell, Sunderam, and Viceira (2013), Adrian and Wu (2009), Hautsch and Ou (2008), Bekker and Bouwman (2009) or Haubrich, Pennacchi, and Ritchken (2012).

we observe differences in the way volatility components comove with liquidity conditions at leads and lags. Since each volatility state that we identify has an economically different interpretation, these results suggest that complex interactions between liquidity and interest rate volatility may be at work.

I. Data

I.A. High-frequency bond data and zero-coupon yield curve tick-by-tick

We use high-frequency nominal US Treasury bond data spanning two long expansions, two recessions and three monetary policy cycles. We obtain 19 years' worth of high-frequency price data of Treasury securities from January 1992 through December 2010 by splicing historical observations from two inter-dealer broker platforms: GovPX (1992:01–2000:12)[4] and BrokerTec (2001:01–2010:12). The merged data set covers about 60% of transactions in the secondary US Treasury bond market. In total, we work with around 50 million on-the-run Treasury bond quotes/transactions (Mizrach and Neely, 2006; Fleming and Mizrach, 2009).

GovPX comprises Treasury bills and bonds with maturities three, six and 12 months, and two, three, five, seven, ten and 30 years. BrokerTec, instead, contains only Treasury bonds with maturities two, three, five, seven (in part of the sample), ten and 30 years. In the GovPX period, we identify on-the-run securities and use their mid-quotes for further analysis. Unlike GovPX, which is a voice-assisted brokerage system, BrokerTec is a fully electronic trading platform attracting vast liquidity and thus allowing us to consider traded prices of on-the-run securities. Roughly 95% of trading occurs between 7:30AM and 5:00PM EST (e.g. Fleming, 1997), which we treat as the trading day. We sample bond prices at ten-minute intervals taking the last available price for each sampling point. More information on our dataset is provided in Appendix I.A

The raw data set contains coupon bonds. We use equally-spaced high-frequency price data to obtain the zero coupon yield curve for every sampling point following the procedure of Fisher, Nychka, and Zervos (1994). In order to anchor the short end of the maturities range in the construction of the zero-coupon curve in the BrokerTec period, we supplement the high-frequency data with the daily observations of the three-month T-bill rate available from the Fed's H.15 statistical release. Even though our zero-coupon yield curve spans

[4] GovPX started operating in 1991.

maturities below two years, in the estimation of realized volatilities we use the two-year yield as the shortest maturity due to the lack of reliable high-frequency data at shorter maturities. Technical details of the zero yield curve construction are delegated to Appendix I.C.

While the availability of the high-frequency data is a restriction on the length of our sample, the 1992–2010 period that we focus on captures a homogenous interest rate environment. There is empirical evidence that the conduct of monetary policy changed significantly during the eighties (e.g., Ang, Boivin, Dong, and Loo-Kung, 2010). The Treasury market functioning has also shifted with the advent of automated trading, and with the rise of the repo, interest rate derivatives and the swap markets.

I.B. Realized yield covariances

The high-frequency zero curve allows us to estimate the realized covariance matrix of yields. We consider two, three, five, seven and ten-year yields, i.e. the most liquid maturities in the secondary bond market (see also Fleming and Mizrach, 2009, Table 1).

Let y_t be the vector of zero yields with different maturities observed at time t. Time is measured in daily units. The realized covariance matrix is constructed by summing up the outer products of a vector of ten-minute yield changes, and aggregating them over the interval of one day $[t, t+1]$:

$$RCov(t, t+1; N) = \sum_{i=1,\ldots,N} \left(y_{t+\frac{i}{N}} - y_{t+\frac{i-1}{N}}\right) \left(y_{t+\frac{i}{N}} - y_{t+\frac{i-1}{N}}\right)'. \tag{1}$$

$N = 58$ is the number of equally spaced bond prices (yields) per day t at the ten-minute sampling, and i denotes the i-th change during the day. For frequent sampling, the quantity (1) converges to the underlying quadratic covariation of yields (Jacod, 1994; Barndorff-Nielsen and Shephard, 2004). The weekly or monthly realized covariances follow by aggregating the daily measure over the corresponding time interval. To obtain annualized numbers, we multiply $RCov$ by 250 for daily, 52 for weekly and 12 for monthly frequency, respectively. In Appendix I.D we verify the robustness of this estimator, and compare it to alternatives proposed in the literature (e.g., Hayashi and Yoshida, 2005). Realized volatility is the square root of the realized variance. Figure 1 plots the zero-coupon yields (panel a) and the realized weekly volatilities (panel b) for maturities of two, five and ten years.

We aim to ensure that our volatility measures reflect the views of active market participants rather than institutional effects. This motivates the following two choices: First, our construction of the *RCov* dynamics relies on the within-day observations, excluding the volatility patterns outside the US trading hours.[5] The second choice lies in focusing on maturities of two years and above. The very short end of the curve (T-bills) is excluded from the realized covariance matrix computations because over our sample period this segment exhibited a continuing decline in trading activity, with data available only till March 2001.[6] Moreover, its dynamics is confounded by interactions with the LIBOR market and monetary policy operations. Such distortions are not directly relevant to the analysis we perform.

I.C. Implied rate volatilities

We obtain implied volatilities from end-of-day prices of individual interest rate options on two-, five- and ten-year Treasury bond and note futures and the corresponding underlyings from the Chicago Mercantile Exchange (CME). For maturities of five and ten years we are able to construct implied volatilities covering the entire 1992–2010 period. In the early part of the sample, the data on the two-year Treasury option is sparse; therefore for this maturity we can reliably construct implied volatilities beginning in March 2006. The underlying of the option is futures on a hypothetical Treasury bond or note that pays coupons. While we refer to the implied volatility by the maturity of the underlying bond, in the model estimation below, we convert them to zero-coupon equivalent. We use options that are closest to at-the-money and one-month maturity, as these are the most active part of the market. Implied volatilities are obtained using the Black's model. The at-the-money implied volatility provides an accurate approximation to the risk neutral expectations of the yield volatility during the following month (e.g. Carr and Wu, 2006). For analogy with the

[5] We observe several abrupt spikes in the between-day volatility, which we cannot relate to any major news in the US market. To account for the total magnitude of volatility, we add to the within-day number the squared overnight yield change from close (5:00PM) to open (7:30PM). We then compute the unconditional average of the total and within-day realized yield covariation, respectively, and each day scale the within-day *RCov* dynamics by the total-to-within ratio. This procedure follows Andersen and Benzoni (2010).

[6] That is when the GovPX sample ends and we switch to using the BrokerTec database. The BrokerTec platform does not cover trading in bonds with maturities below two years. Alternatively, to cover the short maturity segment of the market one could consider using high frequency T-bill futures. However, in the last decade the data becomes sparse. The daily number of trades in the TB contract at the CME has consistently fallen over our sample period, reaching as few as 5 trades per day on average in 2003. For this reason, standard sources of high frequency data stopped supplying T-bill futures after 2003 quoting as a cause a very low secondary market activity in these instruments (e.g. Tickdata.com).

realized yield volatilities, we report annualized implied volatilities on a yield basis. This convention is also followed by the bond market volatility benchmark index, the Merrill Option Volatility Estimate (MOVE), which aggregates implied volatilities across a range of bond maturities.[7] Panel *c* of Figure 1 plots the implied volatilities for two-, five- and ten-year maturities and superimposes them with the MOVE index. Details about options data, conversions and robustness of the implied volatility series are contained in Appendix I.E.

I.D. Empirical facts about interest rate volatility

Table 1 reports summary statistics for the zero-coupon yields (panel A), realized and implied volatilities (panel B), and unconditional correlations between yields and realized volatilities, as well as realized and implied volatilities (panel C).

Factors in volatilities. The principal component analysis suggest that, similar to yield levels, also realized yield volatilities can be described by three factors. The first three principal components explain 90%, 7% and 1.5% of the realized volatilities with maturities between two- and ten-years. Their loadings resemble the level, slope and curvature and are plotted in Figure 2. The recent financial crisis emphasizes the multivariate structure dynamics of yield volatilities. As seen in panel *b* of Figure 1, while the two-year realized volatility increased already during the summer 2007, the ten-year volatility remained relatively low until the Lehman collapse. Following the extraordinary measures undertaken by the Fed and the US Treasury, and the promise of low rates for an "extended period of time," the two-year realized volatility fell sharply in the beginning of 2009, and reached all-time low in the second half of 2010. At the same time, the ten-year volatility remained at elevated levels, perhaps coinciding with the uncertainty about the long-term economic outlook.

Link between interest rates and volatilities. Much of the theoretical and empirical evidence points to a link between the level of interest rates and their volatility. Affine or quadratic models, for instance, imply that the same subset of factors determines both yields and their volatilities. As one example, a single-factor CIR model suggests that the volatility is high whenever the short rate is high (Cox, Ingersoll, and Ross, 1985). While the

[7] MOVE is a weighted index of implied volatilities of one-month options on Treasury bonds. The maturities are weighted as follows: 20% two-year, 20% five-year, 40% ten-year and 20% 30-year bond. These allocations are based on the estimates of option trading volumes in each maturity segment. Options are written on cash bonds rather bond futures. Bond options are traded on an OTC basis, and are therefore less liquid. The data is available only from proprietary sources such as large broker dealers.

CIR-type prediction remained valid through the early 1980s (Chan, Karolyi, Longstaff, and Sanders, 1992), more recently the unspanned stochastic volatility (USV) literature has argued that the yield-volatility relation is weak (Collin-Dufresne and Goldstein, 2002; Andersen and Benzoni, 2010). Using realized volatility we find that this relationship can in fact be nonlinear.[8] The shape of a nonparametric regression fitted to the data suggests a slightly asymmetrically U-shaped pattern: volatility is low for intermediate maturities, and increases when rates move toward either extreme, more so when interest rates become low. Naturally, after the short rate reaches the zero lower bound during the recent crisis, the volatility at the short end of the curve also dies out. Outside this special interest rate environment, the rise in volatility is more pronounced in low interest rate regimes than it is in high interest rate regimes. This is reflected in the negative unconditional correlations between yields and volatilities reported in panel C of Table 1.

Figure 3 plots average yield and realized volatility curves conditional on the monetary policy stance (easing, tightening or no action).[9] A monotonically increasing average term structure of yields is accompanied by a humped term structure of volatilities, with the hump most pronounced at the three-year maturity during easing episodes. In our sample, a monetary policy easing is associated with a rising slope of the yield curve, a higher level of yield volatility and an increased magnitude of the volatility hump.

Implied vs realized volatilities. Table 1 shows that on average, and most visibly at the short maturity, implied volatilities exceed realized volatilities, suggesting a negative volatility risk premium. For the two- and five-year maturity, the difference between the implied and realized yield volatilities is about 22 and 14 basis points, respectively. Relative to the realized volatilities, implied volatilities are more persistent and have a lower unconditional standard deviation. The bottom panel of Table 1 reports unconditional correlations between realized and implied volatilities and the MOVE index. The lowest correlation reaches 0.51 between the ten-year implied and two-year realized volatility. The correlation between MOVE and our implied volatility series exceeds 0.9, except for the two-year maturity where we cover only a short part of the sample. At the weekly frequency, the three principal components of realized volatilities explain between 45% and 49% of variation in implied volatilities across maturities. Given that there is a lot of high-frequency variation in realized volatilities,

[8] The results summarized here are not reported in any table for brevity.

[9] A period is classified as easing, tightening or no action (stay) if it spans at least three subsequent moves in the federal funds rate target in a respective direction.

this share increases to between 68% and 72% when we smooth realized volatilities with a four-week moving average.

II. The model

We propose a no-arbitrage model for the joint dynamics of nominal yields and their time-varying second moments. The model introduces multiple factors in yield volatilities, and allows for priced yield and volatility risks. We use the model to decompose and analyze the variation in the covariance matrix of yields in a way that is consistent with a small number of factors in the term structure, and in particular the components of short rate expectations and the term premia. The model also allows us to study the role of yield volatilities for the cross section of yields and for the bond risk premia.

II.A. The no-arbitrage framework

We distinguish between yield curve factors X_t, and covariance factors V_t. The physical dynamics are given by the system:

$$dX_t = (\mu_X + \mathcal{K}_X X_t)dt + \sqrt{V_t}dZ^{\mathbb{P}}_{X,t} \quad (2)$$

$$dV_t = (\Omega\Omega' + MV_t + V_tM')\,dt + \sqrt{V_t}dW^{\mathbb{P}}_t Q + Q'dW^{\mathbb{P}\prime}_t\sqrt{V_t}, \quad (3)$$

where X_t is a n-dimensional vector, and V_t is a $n \times n$ covariance matrix process (Bru, 1991; Gourieroux, Jasiak, and Sufana, 2009); $Z^{\mathbb{P}}_X$ and $W^{\mathbb{P}}$ are an n-dimensional vector and a $n \times n$ matrix of independent Brownian motions, respectively; μ_X is a n-vector of parameters and $\mathcal{K}_X, M$ and Q are $n \times n$ parameter matrices.[10]

We consider a setup in which $n = 2$, i.e. X_t contains two factors with a time-varying conditional covariance matrix. Since we do not model the time-varying second moments at the shortest maturity range, we introduce a third yield curve state f_t evolving as:

$$df_t = (\mu_f + \mathcal{K}_{fX}X_t + \mathcal{K}_f f_t)dt + \sigma_f dZ^{\mathbb{P}}_{f,t}. \quad (4)$$

$\mathcal{K}_f$ and σ_f are scalars, $\mathcal{K}_{fX}$ is a 1×2 vector, and $Z^{\mathbb{P}}_{f,t}$ is a Brownian motion independent of all other shocks in the economy. As such, X_t can impact the conditional expectation of f_t

[10] To ensure a valid covariance matrix process V_t, we specify $\Omega\Omega' = kQ'Q$ with an integer degrees of freedom parameter k such that $k > n - 1$, and require that Q is invertible. This last condition guarantees that V_t stays in the positive definite domain (see e.g., Gourieroux, 2006).

through the drift. Time-varying volatility enters the model through V_t that describes the amount of risk in the economy, with off-diagonal elements of V_t determining the conditional covariance between X_t's. We focus on modeling the stochastic covariance of yields of intermediate to long maturities, whose variation we can observe with support of high frequency data. Given the different institutional properties of shortest maturity yields and the unavailability of traded high-frequency data, we assume constant conditional volatility for f_t.

We collect X_t and f_t factors in a vector $Y_t = (X_t', f_t)'$, whose dynamics can be compactly written as:

$$dY_t = (\mu_Y + \mathcal{K}_Y Y_t)\, dt + \Sigma_Y(V_t) dZ_t^{\mathbb{P}}, \tag{5}$$

where $\Sigma_Y(V_t)$ is a block diagonal matrix with $\sqrt{V_t}$ and σ_f on the diagonal, and $\mathcal{K}_Y = \begin{pmatrix} \mathcal{K}_X & 0_{n\times 1} \\ \mathcal{K}_{fX} & \mathcal{K}_f \end{pmatrix}$.

The short interest rate is an affine function of X_t and f_t:

$$r_t = \gamma_0 + \gamma_X' X_t + \gamma_f f_t = \gamma_0 + \gamma_Y' Y_t \tag{6}$$

with $\gamma_Y = (\gamma_X', \gamma_f)'$.

Bonds are priced by no-arbitrage. We specify the stochastic discount factor as:

$$\frac{d\xi_t}{\xi_t} = -r_t dt - \Lambda_{Y,t}' dZ_t^{\mathbb{P}} - Tr\left(\Lambda_{V,t}' dW_t^{\mathbb{P}}\right), \tag{7}$$

with market prices of risk:

$$\Lambda_{Y,t} = \Sigma_Y^{-1}(V_t)\left(\lambda_Y^0 + \lambda_Y^1 Y_t\right) \tag{8}$$

$$\Lambda_{V,t} = \left(\sqrt{V_t}\right)^{-1} \Lambda_V^0 + \sqrt{V_t}\Lambda_V^1. \tag{9}$$

This specification assumes that shocks to both yield and volatility factors are priced, preserving the tractable affine structure of the model. The market price of risk parameters have the following dimensions: $\lambda^0_{Y,(3\times 1)}$, $\lambda^1_{Y,(3\times 3)}$, $\Lambda^0_{V,(2\times 2)}$, and $\Lambda^1_{V,(2\times 2)}$. Equation (8) follows Duffee (2002)'s essentially affine market price of risk. Equation (9) is an analogous extension for the volatility states.

Prices of nominal bonds are obtained by solving $P_t^\tau = E_t^{\mathbb{Q}}\left(e^{-\int_0^\tau r_s ds}\right)$. The solution for the nominal term structure has an affine form:

$$P(t,\tau) = \exp\{A(\tau) + B(\tau)'Y_t + Tr\left[C(\tau)V_t\right]\}, \tag{10}$$

where $Tr(\cdot)$ denotes the trace operator. The coefficients $A(\tau), B(\tau)$ and $C(\tau)$ solve a system of ordinary differential equations:

$$\frac{\partial A(\tau)}{\partial \tau} = B(\tau)'\mu_Y^{\mathbb{Q}} + \frac{1}{2}B_f^2(\tau)\sigma_f^2 + Tr\left[\Omega^{\mathbb{Q}}\Omega^{\mathbb{Q}}C(\tau)\right] - \gamma_0 \tag{11}$$

$$\frac{\partial B(\tau)}{\partial \tau} = K_Y^{\mathbb{Q}\prime}B(\tau) - \gamma_Y \tag{12}$$

$$\frac{\partial C(\tau)}{\partial \tau} = \frac{1}{2}B_X(\tau)B_X(\tau)' + C(\tau)M^{\mathbb{Q}} + M^{\mathbb{Q}\prime}C(\tau) + 2C(\tau)Q'QC(\tau), \tag{13}$$

where $K_Y^{\mathbb{Q}}$, $M^{\mathbb{Q}}$ and $\Omega^{\mathbb{Q}}$ are the parameters of the risk neutral dynamics. We split the $B(\tau)$ loadings as $B(\tau) = [B_X(\tau)', B_f(\tau)]'$. The boundary conditions for the system (11)–(13) are $A(0) = 0_{1\times1}, B(0) = 0_{3\times1}$ and $C(0) = 0_{2\times2}$. $B(\tau)$ has a standard solution as in Gaussian models; $C(\tau)$ solves a matrix Riccati equation. All technical details are collected in Appendix II.

Defining $y_t^\tau = -\frac{1}{\tau}\ln P_t^\tau$, the term structure of interest rates is obtained as:

$$y_t^\tau = -\frac{1}{\tau}\{[A(\tau) - B(\tau)'Y_t - Tr\left[C(\tau)V_t\right]\}. \tag{14}$$

The instantaneous yield covariation is only driven by the covariance factors, V_t:

$$\begin{aligned} v_t^{\tau_i,\tau_j} &:= \frac{1}{dt}\langle dy_t^{\tau_i}, dy_t^{\tau_j}\rangle \\ &= \frac{1}{\tau_i\tau_j}\{Tr\{[B_X(\tau_i)B_X(\tau_j)' + 4C(\tau_i)Q'QC(\tau_j)]\,V_t\} + B_f(\tau_i)B_f(\tau_j)\sigma_f^2\}, \end{aligned} \tag{15}$$

and the conditional risk-neutral expectation of the annualized yield variance over horizon h is:

$$v_{t,t+h}^{\mathbb{Q},\tau} = E_t^{\mathbb{Q}}\int_0^h v_{t+s}^\tau ds, \tag{16}$$

which is available in closed form but omitted from the main text for brevity. Analogously, $v_{t,t+h}^{\mathbb{P},\tau}$ is the expected h-period variance under the physical dynamics.

The model implies that the instantaneous expected return, brp_t^τ, to holding a bond with maturity τ is:

$$brp_t^\tau = \left(\lambda_Y^0 + \lambda_Y^1 Y_t\right)' B(\tau) + 2Tr\left[(\Lambda_V^0 + \Lambda_V^1 V_t) Q C(\tau)\right]. \tag{17}$$

The first term in (17) is common with the Gaussian dynamic term structure models (DTSMs), the second term is a new element that captures the effect of volatility on the bond risk premia. Thus, volatility states are allowed to affect both the levels of yields in equation (14) and the bond risk premia in (17). The variance risk premium, defined as the difference between the expected h-period variance under the physical and risk neutral dynamics:

$$vrp_{t,t+h}^\tau = v_{t,t+h}^{\mathbb{Q},\tau} - v_{t,t+h}^{\mathbb{P},\tau} \tag{18}$$

is determined by the volatility states V_t and the corresponding market price of risk parameters in equation (9).

II.B. Discussion

Our distinction between volatility and yield curve states builds on the $A_m(n)$ classification of ATSMs introduced by Dai and Singleton (2000). The new element is that V_t represents a covariance matrix, involving an interaction factor which can change sign.[11] The form of V_t leads to a three-factor model for the second moments of yields with two volatility and a covariance state. This structure helps us to overcome the difficulties of DTSMs in matching conditional volatilities of long-maturity yields reported in the literature. The combination of six factors gives the model the flexibility to fit both yields and volatilities. The state space we consider is large, but involves a relatively small number of identified parameters (13), excluding the market price of risk parameters in (8)–(9).

The presence of V_t in expression (14) distinguishes our model from the unspanned stochastic volatility settings, which impose explicit restrictions so that the volatility factors do not enter the cross section of yields. Such separation usually improves the volatility fit of low-dimensional ATSMs (Collin-Dufresne, Goldstein, and Jones, 2009). However, as highlighted by the literature, there appear to be few reasons, except statistical ones, for such constraint to strictly hold (Joslin, 2007). The volatility variables could appear in the term structure of

[11] In ATSMs, independent CIR processes generate stochastic volatility one-by-one, and therefore conditional covariances they imply are a linear combination of the volatility factors.

yields through at least two channels. One of them is the convexity (e.g. Phoa, 1997). The second one is the effect that volatility has on the risk premia. We explore the importance of these channels below.

II.C. Estimation

We estimate the model on a weekly frequency ($\Delta t = \frac{1}{52}$) combining pseudo-maximum likelihood with filtering. All technical details on the estimation and identification are presented in Appendix III.A.

We introduce three types of measurements for yields ($\tilde{y}_t^\tau$), their quadratic covariation ($\tilde{v}_t^{\tau_i,\tau_j}$) and the expected risk neutral variance over the next month ($\tilde{v}_{t,t+4}^{\mathbb{Q},\tau}$):

$$\tilde{y}_t^\tau = f_1(Y_t, V_t; \Theta) + \sqrt{R_1} e_{1,t} \tag{19}$$

$$\tilde{v}_t^{\tau_i,\tau_j} = f_2(V_t; \Theta) + \sqrt{R_2} e_{2,t} \tag{20}$$

$$\tilde{v}_{t,t+4}^{\mathbb{Q},\tau} = f_3(V_t; \Theta) + \sqrt{R_3} e_{3,t}. \tag{21}$$

Functions $f_i(\cdot), i = \{1, 2, 3\}$ denote the model-implied expressions corresponding to the measurements; Θ collects model parameters. $\tilde{v}_t^{\tau_i,\tau_j}$ is obtained from the high-frequency zero-coupon yield curve using the realized covariance estimator (1). The expected risk neutral variance $v_{t,t+4}^{\mathbb{Q},\tau}$ is identified from the squared implied volatility series.

We assume additive, normally distributed measurement errors $e_i, i = \{1, 2, 3\}$ with zero mean and a constant covariance matrix. In estimation, we use six yield measurements with maturities of six months and two, three, five, seven and ten years with $R_1 = \sigma_y^2 I_{(6\times6)}$, where $I_{(6\times6)}$ is an identity matrix, and σ_y is common across maturities. We include four realized variance measurements: realized variances of the two-, five- and ten-year bond and the covariance between the five- and ten-year bond, as well as three measurements for the risk neutral variance with underlying bond maturities of two, five and ten years. The two-year implied volatility is available only in part of the sample, therefore in estimation we treat the initial observations as missing. Since our implied volatility series have coupon bonds as the underlying, we use the average duration of the bond during our sample period to obtain the zero-coupon implied volatility equivalent. The implied volatility measurements are therefore matched with the model-based risk neutral volatility $v_{t,t+4}^{\mathbb{Q},\tau}$ with $\tau = 1.9$, 4.4 and 7.5 years, respectively.[12] In total, we have seven variance measurements, and for each

[12] These numbers represent the average duration of the underlying coupon bond in our sample.

we allow a different measurement error, i.e. R_2 and R_3 are diagonal matrices with four and three parameters, respectively.

In order to handle the non-Gaussianity in factor dynamics we use the square-root Unscented Kalman Filter (UKF), proposed by Julier and Uhlmann (1997).[13] We maximize the likelihood with the global optimization algorithm of Price, Storn, and Lampinen (2005).

Finally, we impose parameter restrictions that ensure econometric identification of the model. After that, the baseline model has 13 parameters which drive the yield curve (six of which describe the market prices of risk), and ten parameters which drive the volatilities (four of which describe the market price of risk).

III. Empirical results

This section uses the model to analyze the empirical properties of interest rate volatility. First, we discuss a decomposition of volatility into a short rate expectations component and a term premium component. Second, we study how volatility affects the yield curve and the level the bond risk premia.

III.A. Estimated factors

The model fits the data well indicating that it has the flexibility to summarize information in yields, and in realized and implied volatilities. A summary of the model's performance is provided in Appendix IV.

Figure 4 plots the model-implied factor dynamics. Panels on the left display the evolution of the yield curve factors $Y = (X_1, X_2, f)$, those on the right show the corresponding volatility states $\bar{V} = (V_{11}, V_{21}, V_{22})$,[14] capturing the conditional covariance of the yield curve factors X_1 and X_2.

Figure 5 shows how these factors affect the yield curve. Each line presents the model-implied factor loadings in equation (14), scaled by one standard deviation of each factor. Panel *a* displays the $B(\tau)$ coefficients. The effect of f_t is most pronounced at the short end of the yield curve. The time series of f_t in Figure 4 suggests that this factor closely traces

[13] See e.g. Carr and Wu (2007) and Christoffersen, Jacobs, Karoui, and Mimouni (2009) for the recent applications of the unscented Kalman filter to asset pricing.

[14] We rotate the yield curve factors such that their increase has a positive effect on the yield curve. In practice this amounts to multiplying X_2 by -1. Correspondingly, the sign of the covariance state V_{21} is switched. Other than convenience, these adjustments have no implications for the results.

the short-maturity rates: its correlation with the the Fed funds target is 0.96. In that narrow correlation sense, f_t reflects the stance of the monetary policy within the model. The two remaining factors influence the longer segment of the yield curve: the impact of X_1 increases with the maturity, while X_2 affects most strongly the short-to-intermediate maturities between two and three years.

The volatility factors in panel b behave accordingly: the effect of V_{11} on interest rate volatility rises whereas that of V_{22} declines with the maturity. Respectively, we label them as the long-end and the short-end volatility. The V_{21} term drives the conditional covariance between the yield curve factors. The estimated dynamics suggest that the covariance state changes sign during our sample period.

As visible in the right-hand panels of Figure 4, the estimates of the V_t process imply that the long- and short-end volatility have different time series properties. Not surprisingly, volatility states are substantially less persistent than the yield curve states. A less immediate observation is that the short-end volatility is less persistent than the long-end. The half-lives under the real world ($\mathbb{P}$) dynamics are below one year (47 weeks) for the short-end volatility V_{22} and above 1.5 years (90 weeks) for the long-end volatility V_{11}.

III.B. Volatility of term premia versus volatility of short rate expectations

Our factors are latent, and therefore they are not directly linked to any observable macro quantities. However, the structure of the model allows us to analyze the interactions between well-defined economic quantities in the yield curve.

Yield volatility stems from either volatile short rate expectations, or volatile term premia, and comovement between the two (plus a convexity-related term). If interest rates become more volatile, one would like to understand which component contributes to the volatility increase. To the extent that short rate expectations reflect expectations about the future path of monetary policy, their volatility can be informative about the amount of uncertainty surrounding that path at different horizons. The conclusion that we draw from this section is that the model-based volatility factors have separate interpretations in terms of their link to short rate expectations and term premia.

We compute the conditional volatilities associated with:

$$r^e_{t,t+\tau} = \frac{1}{\tau} E^{\mathbb{P}}_t \left(\int_0^\tau r_{t+s} \right) ds \tag{22}$$

$$rpy^\tau_t = \frac{1}{\tau} \left[E^{\mathbb{Q}}_t \left(\int_0^\tau r_{t+s} \right) ds - E^{\mathbb{P}}_t \left(\int_0^\tau r_{t+s} \right) ds \right], \tag{23}$$

where $r^e_{t,t+\tau}$ denotes the expected average short rate, and rpy^τ_t is the term premium. These expressions are affine in V_t and have a tractable form provided in Appendix V.

Figure 6 shows how volatility states contribute to the second moments of short rate expectations (panel a) and risk premium (panel b) across maturities. The loadings reveal an interesting distinction. The long-end volatility, V_{11}, emerges as the dominant factor for the variance of the term premium, but it has a minimal contribution to the variance of short rate expectations.[15] The short-end volatility, V_{22}, does the opposite: While its impact on the term premium part is effectively zero, this factor plays a key role in generating the variance of short rate expectations. It seems justified to label these factors as the term premium and short rate expectations volatility, respectively. Below, we use interchangeably the terms short-end (long-end) volatility and short rate expectations (term premium) volatility. The covariance state contributes to both, but its effect on the short rate expectations component is stronger, suggesting that an increase in the comovement between yields across maturities makes short rate expectations more volatile.

Panels c and d in Figure 6 plot the time series of volatilities of expectations and of term premia for the two-year (panel c) and the ten-year yield (panel d). The volatility of the two-year bond is dominated by the expectations part, while that of the ten-year bond—by the term premium part, even though the volatility of short rate expectations still plays a significant role at the ten-year maturity. This evidence is consistent with a scenario in which short rate expectations are mean reverting, and their effect declines with the maturity, i.e. the Fed has a limited control over the long-end of the yield curve; this is accompanied by an increasing role of the term premium at the longer maturities range.

Given their different interpretation, it is useful to study the behavior of volatility states over the business cycle. Figure 7 displays the evolution of long- and short-end volatility in our sample. Consistent with its link to short rate expectations, the short-end volatility typically rises before recessions, perhaps on an increased uncertainty about an upcoming monetary policy easing; in those episodes the long-end (term premium) volatility remains

[15] The one factor structure for the volatility of the term premium agrees with the result in the literature that bond risk premia move on a single factor (e.g. Cochrane and Piazzesi, 2005).

contained. After recessions both tend to rise. This is the case for each post-recession period in our sample: in 1992 (post 1990–1991 recession) the long-end volatility increased by more than three standard deviations away from its unconditional mean; similarly in 2003 (post 2001 recession) it moved almost four standard deviations from the mean. The short-end volatility factor exceeds the four standard deviations mark five times in our sample all of which concur with monetary policy easings. It also increases during periods of distress in asset markets such as the LTCM, the Russian crisis or the dot-com bubble, which in the 1990s and 2000s have been paired with supportive monetary policy actions. During the recent financial crisis, the short-end volatility reached extreme levels already in the Fall 2007 and persisted until 2009. The long-end volatility, instead, remained low until the bankruptcy of Lehman Brothers, after which it peaked in March 2009. Given its interpretation as the term premium volatility, one could view this as a sign of the bond market being concerned about the consequences of fiscal and non-standard monetary policy measures for the future risk of Treasuries. We provide evidence supporting this intuition in Section IV.

III.C. Comovement between term premia and short rate expectations

From the monetary policy perspective, one important reason for studying the second moments of yields is the question of how short rate expectations and risk premia comove over time. For instance, a negative comovement in an easing environment may suggest that the Fed faces a tradeoff between lowering short term interest rates to stimulate the economy, and increasing the inflation risk premium. By modeling directly the stochastic covariance of risks, our setting is uniquely suited to study the empirical properties of this tradeoff.

Panel *e* in Figure 6 displays the role of the model-implied factors in generating the comovement between shocks to the term premia and to short rate expectations. To obtain the loadings, we compute the conditional covariance of the two objects in equations (22) and (23). Consistent with its interpretation as the covariance state, the figure shows that the V_{21} factor has the largest impact on the covariance, which increases upon a positive shock to the factor.

Panel *f* in Figure 6 plots the conditional correlation between the shocks to risk premia and to short rate expectations implied by the model for maturities of two and ten years. Two features of that correlation are important: First, during our sample period, the correlation

is low on average and positive, with its unconditional mean reaching 0.14 for two-year bond and 0.21 for the ten-year bond. Second, the correlation is persistent but clearly time-varying, changing sign multiple times during our sample. In the plot, we superimpose its dynamics with the Fed funds target (rescaled to fit the graph). On average, the correlation between risk premia and expected short rates increases during easings and declines during tightenings. Interestingly, the model interprets the Greenspan's conundrum period, i.e. the lack of response of long-term yields to the Fed's 2004/05 tightening, as a decline in the correlation between the expected short rate and the term premium from nearly one to negative -0.4.

The evolution of the tradeoff between expected short rates and the term premia, along with their low unconditional correlation, casts new light on the view that in the last two decades the link between short- and long-term interest rates has been largely severed (e.g. Thornton, 2012).

III.D. Additional model implications

This section focuses on the channels through which volatility impacts the yield curve. We find that in terms of modeling the cross-section of interest rates, analyzing priced sources of risk in the term structure, and the time-varying bonds risk premia, the conclusions from the model with a rich second moments dynamics are close to these based on a Gaussian setting. At the same time, in Section IV we show that modeling interest rate volatility is not a void exercise, in that volatility states contain information about the economy that cannot be extracted from yields themselves.

III.D.1. Implications for the Treasury risk premia

Expression (17) shows that the model-based bond risk premia have two components loading on the yield curve and volatility states, respectively. Abstracting from the time-varying second moments in Y_t, the first component arises similarly in Gaussian models and we will refer to is as the Gaussian part of the bond risk premium. The second component is a consequence of the priced volatility risk in the Treasury bond market, i.e. the variance risk premium. We investigate the amount of time-variation in bond excess returns due to each element. The model implies that during our sample period the variance risk premium does not contribute significantly to the predictability of returns on Treasury bonds.

The results are collected in Table 2. We compute the model-implied expected bond excess returns for an annual holding period which is the horizon customarily used in the literature on bond return predictability. We then regress the realized excess returns from the data on the model-implied risk premia. We consider three variants of the regressions. Panel A is based on the total model-implied risk premium; panel B involves only the Gaussian part and zeros out the risk premium variation due to the volatility states. Panel C benchmarks the model-based results to the predictability obtained with the return forecasting factor of Cochrane and Piazzesi (2005, CP). In our sample, the CP factor predicts between 8% and 19% of the variation in the annual realized excess returns at maturities between two and ten years. The model-based risk premium gives a slightly lower degree of predictability ranging between 3% and 13%.[16] A comparison of panels A and B of the table suggests that priced volatility risk does not contribute in a significant manner to the predictable variation of bond excess returns.

One may wonder how this conclusion depends on the return horizon that we predict. Given the impersistent nature of yield volatility, one could expect the effect of volatility states on the risk premium to be material only at short horizons. Panel D and E of Table 2 present results analogous to the above regressing the realized returns with a holding period of one month onto the instantaneous model-based risk premium. The results appear to confirm the previous conclusion that the contribution of the priced variance risk to the bond risk premium is minute.

However, the model implies a non-zero variance risk premium: on average, investors pay a premium for the volatility protection. The variance risk premium defined in equation (18) has a slightly humped pattern across maturities, is the highest at the maturity of three years, and declines with maturity. In basis points terms, the model implies the volatility risk premium, measured as the average of $\sqrt{v^{\mathbb{Q},\tau}_{t,t+h}} - \sqrt{v^{\mathbb{P},\tau}_{t,t+h}}$ with $h = 4$ weeks, equal to 21 (22.5) basis points at the two-year (three-year) maturity and less than 9 basis points at the ten-year maturity. In that yield volatility at short maturities is mostly driven by the volatility of short rate expectations, it seems plausible that the variance risk premium

[16] At longer maturities, the realized excess returns load on the model-based risk premia with a slope coefficient that exceeds one, suggesting that risk premium from the model is less volatile than the data. The non-unit coefficient may be a consequence of our relatively short sample period. We can reject the non-unit coefficient only for maturities of nine and ten years at the 5% level. Using survey data to measure expected excess bond returns on the two-year bond we also find a non-unit (and insignificant) coefficient and a $\bar{R}^2$ of about 3%.

reflects mainly a compensation for the risk related to volatile expectations about monetary policy.

III.D.2. Role of volatility in the cross-section of yields

A question that has attracted attention is how volatility affects the cross section of interest rates. Quantifying this effect requires a model that is rich enough to accommodate the empirical properties of both the first and second moments of yields. The literature summarized in the introduction argues that standard dynamic term structure models lack the flexibility to generate realistic yield volatilities, especially at the long end of the term structure. Therefore, potential misspecification complicates a model-based inference about the linkages between yields and volatilities. Our approach is different in that we equip the model with a multifactor structure that the data calls for but also ask it to actually match the observed second moment dynamics.

Panel *c* of Figure 5 uses equation (14) to measure how the shape of the term structure changes when the volatility changes. The graph makes clear that this channel is quantitatively small. Even a two standard deviation shock to volatilities has a total (negative) impact on the ten-year yield of about eight basis points. It is almost entirely driven by the long-end (term premium) volatility state and, consistent with the usual convexity effect, most visible at long maturities. Interestingly, we find that the short-end volatility related to short rate expectations is essentially impossible to uncover from the cross-section of yields: Its corresponding yield-curve loadings are effectively zero. As such, using terminology of Duffee (2011), this factor can be interpreted as hidden. In contrast to the USV models, this result is obtained without imposing constraints on the model parameters that would prevent a priori the volatility states from entering the cross section of yields.

III.E. Comparison with a volatility-only model

To better understand the role of no-arbitrage restrictions for our results, we estimate a stochastic volatility model that does not impose any consistency requirements on the joint dynamics of yields and volatilities. Specifically, we estimate a stand-alone volatility process given by equation (3) using the same volatility measurements as in the case of our term structure model. Parameter estimates are not reported for brevity. Table 3 provides cross-correlations between the volatility factors obtained from the two approaches. The highest correlation of 0.7 pertains to the short-end volatility, while that for the long-end volatility

is below 0.3. This suggests that the no-arbitrage restrictions are useful in disentangling the volatility of short rate expectations from the volatility of the risk premia. The stronger correlation of the short-end volatility is consistent with short rate expectations driving a higher share of the overall volatility in yields. Figure 9 shows that the largest differences between factors implied by these two settings arise during recessions. While the short- and long-end volatility factors from the no-arbitrage model increase in different recession phases, the factors in the volatility-only model move much more in sync during downturns. For comparison, Table 3 also reports correlations with the first three principal components of the realized and implied yield volatilities. The volatility states from the no-arbitrage model have a significantly weaker relationship to the principal components than those from the volatility-only model.

IV. A macro-finance link

This section verifies our interpretation of yield volatility factors by linking them to observable uncertainty proxies. We also show that interest rate volatility, and in particular the volatility of short rate expectations, provides new information about the economy that is not contained in the standard yield curve factors.

IV.A. Macroeconomic uncertainty

We relate volatility factors from the model to survey-based proxies for expectations and uncertainties about the macroeconomy. Forecasts of macro variables are from the Blue Chip Financial Forecasts (BCFF). As documented in the transcripts of the FOMC meetings, these surveys are regularly used by policymakers at the Fed to read market expectations.[17] Appendix I.F provides details about the survey data including their timing within a month. We use responses of individual panelists to construct proxies for the consensus forecast and for the uncertainty. Each month, the consensus is computed as the median survey reply. Uncertainty is measured with the mean absolute deviation of individual forecasts.[18] We consider forecasts of the real GDP growth (RGDP), the federal funds rate (FFR) and all-items CPI inflation (CPI). For each variable and each month we have a term structure

[17] Between 1994 and 2007, the FOMC transcripts refer to the forecasts from the Blue Chip survey 146 times during 61 FOMC meetings.

[18] Disagreement in survey forecasts could be more reflective of differences of opinions rather than uncertainty (Diether, Malloy, and Scherbina, 2002), so we do not draw a sharp distinction between the two notions, but we assume that they are correlated.

of forecasts from the current quarter out to four quarters ahead. To summarize this information, we compute the average consensus/uncertainty across horizons. We also relate yield volatility to the economic policy uncertainty index constructed by Baker, Bloom, and Davis (2013, BBD).

We run contemporaneous regressions of model-based volatility states on the above variables. Since consensus forecasts can be very persistent, given our relatively short sample, we use their monthly changes rather than levels. Table 4 summarizes the results for the 1992–2010 sample (panel A), and for the 1992–2007 sample excluding the recent crisis (panel B). For the full sample, we capture between 38% and 42% of variation in the yield volatility states and about 14% in the covariance state. These shares remain similar in the 1992–2007 sample. The three volatility states differ in the way they load on the explanatory variables. In terms of macro consensus, the long-end volatility is positively related to the changes in the expected RGDP. This link is most visible during the recent crisis, where the long-end volatility factor peaked *after* growth expectations started to recover from the bottom of the recession.[19] One interpretation of the positive sign is that despite the initial signals of recovery, the long-end volatility has moved up on concerns about long-term consequences of the fiscal and monetary stimulus. The model associates this pattern with an increased volatility of the term premia. We find support for this interpretation based on the policy uncertainty index below. The short-end volatility, instead, comoves negatively with changes in the monetary policy measured with the FFR. A 50 basis points negative change in the expected FFR raises the short-end volatility by approximately a half standard deviation.

Both short- and long-end volatility increase with the uncertainty about the real economy. The most important difference between them is that the short-end volatility comoves positively with the level of uncertainty about the FFR, while the long-end volatility—with the economic policy uncertainty as measured with the BBD index. This distinction aligns well the interpretation of these factors as the volatility of short rate expectations and term premia, respectively. It is also interesting in the context of the findings of BBD, who argue that their index reflects mainly uncertainties about taxes, spending as well as monetary and regulatory policies. In particular, they find that since 2008 the increases of the index have been dominated by the elevated tax, spending and regulatory concerns, but not concerns about the Fed. This is supported with the behavior of the yield volatility

[19]The relationship between the long-end volatility and the growth rate of real activity is complex in that overall the long-end volatility increases in recessions, but it does so at the recession exit when real activity indicators (e.g. CFNAI) have already bottomed and show first signs of recovery.

states just before and during the crisis (see Figure 7): The short-end volatility increased already in 2007 and then declined ahead of the long-end volatility, while the latter remained low until mid-2008, rose afterwards and remained high through the end of our sample in 2010. A projection of the policy uncertainty index on the volatility states (not reported in any table for brevity) reveals that the index covaries most strongly with the short-end volatility before the crisis, and with the long-end volatility from 2007 onwards. Thus, the behavior of the model-based volatility factors and their respective links to the Fed and to the economic policy uncertainties suggest that these factors distill and trace consistently over time particular types of risk.

It is worth noting that the covariance state has the weakest relation to the survey-based consensus and uncertainty measures. To the extent that it drives the comovement between the term premium and short rate expectations, linear regressions like the ones we estimate above may not be appropriate to capture the information this factor contains. However, we find that covariances between realized macro variables and interactions between survey-based uncertainty measures are able to explain up to 33% of its dynamics, with the interaction of uncertainty about the FFR and the CPI being the most significant one.

IV.B. Forecasting growth

The literature has documented that the slope of the yield curve has predictive power for the economic activity: a higher slope predicts an increase in the real activity, consumption and investment at horizons between one and two years ahead (Estrella and Hardouvelis, 1991; Harvey, 1989). We show that there is additional information in yield volatility over and above that contained in the cross section of yields.

We forecast economic activity, measured with the CFNAI (Chicago Fed National Activity Index)[20] by estimating the following regression:

$$\text{CFNAI}_{t+k} = \beta_k' X_t + \varepsilon_{t+k}, \quad k = \{0, 1, \ldots, 24\} \text{ months}, \tag{24}$$

[20]The CFNAI is published on the Chicago Fed web page as a weighted average of 85 existing monthly indicators of national economic activity including (*i*) production and income, (*ii*) employment, unemployment, and hours, (*iii*) personal consumption and housing, and (*iv*) sales, orders, and inventories. The index is constructed to have an average value of zero and a standard deviation of one. Since economic activity tends toward trend growth rate over time, a positive index reading corresponds to growth above trend and a negative index reading corresponds to growth below trend. Thus, we can interpret CFNAI as a growth indicator. We use the monthly unsmoothed reading of the index.

where as explanatory variables in X_t we consider yield curve factors (principal components), and/or volatility states. We predict activity at horizons ranging from the current month through 24 months ahead.

Figure 8 shows the results for different specifications of equation (24). Panel *a* compares the predictive $\bar{R}^2$ obtained from two regressions using as the explanatory variables: (*i*) the three volatility states obtained from the model, and (*ii*) the first four yield PCs. The figure reveals different predictability patterns in the two specifications. While in volatility regressions the highest $\bar{R}^2$s are obtained at short horizons reaching a peak of 37% at $k = 7$ months, the yield PCs regressions give initially low predictability which increases at horizons above one year, and reaches 29% at $k = 24$.

In panel *b*, we repeat the same predictive exercise but using only the short-end volatility V_{22} and the yield curve slope. We find that these two variables account for the main part of the predictability in the previous regressions. The predictive power of the short-end volatility is the highest at $k = 7$ months with $\bar{R}^2$ of 23%. The slope-only regression, instead, gives the maximum predictability at horizons above one year, which is in line with the evidence in the literature, e.g. at $k = 24$ the $\bar{R}^2$ is 25%. In both cases, the regression coefficient is significant at the 1% level.

Panel *c* summarizes bivariate regressions with slope and short-end volatility included jointly. In the plot, we mark horizons for which each regressor is significant at the 1% level. The pattern of coefficients is consistent with the previous graphs suggesting that yield volatility operates at shorter horizons than the slope. Importantly, for all specifications, the short-end volatility has a negative coefficient. Using implications of our model, a rising volatility of short rate expectations is a signal for lower growth several months ahead.

Panel *d* compares the properties of the three volatility factors from our model in terms of forecasting growth, and shows that the short-end volatility dominates the other two factors. The covariance state does not predict activity at all, and the long-end volatility is significant (with a negative coefficient) only in contemporaneous regressions ($k = 0$) and at the long horizon, although we find that this latter result is not robust to the exclusion of the crisis years.

Panel *d* additionally contains the equity market VIX. While both the short-end volatility and the VIX increase in anticipation of bad times, the importance of VIX decays faster with the horizon k, indicating that information about future growth contained in the short-end

volatility is different than that in the VIX. In bivariate regressions (details not reported), both VIX and the short-end volatility remain significant at the 5% level for k up to about nine months (VIX) and one year (V_{22}), and both preserve their negative coefficients.

The forecasting power of the short-end volatility and the slope remains robust to the exclusion of the crisis years. In the pre-crisis sample, the short-end volatility captures up to 17% of variation in the future CFNAI at short horizons. At the same time, with the exclusion of the crisis, the predictive power of VIX becomes significantly weaker.

IV.C. Liquidity measures

Liquidity and the highest quality of collateral are important motives driving demand for the US Treasuries (Krishnamurthy and Vissing-Jorgensen, 2010; Longstaff, 2004). We ask how these motives are related to yield volatility. These results are summarized in Table 5.

We consider several liquidity measures that have been proposed in the literature and which capture multifaceted nature of liquidity. First, we use the Hu, Pan, and Wang (2012, HPW) noise illiquidity, which measures temporary price deviations of Treasury bonds from a smooth yield curve. HPW show that the illiquidity is related to the availability of arbitrage capital in the market. An increase in illiquidity signals that arbitrage capital becomes scarce and the overall market liquidity deteriorates.

As a second measure, we consider the systematic liquidity factor in the equity market from Pastor and Stambaugh (2003, PS). A lower value of the PS factor indicates a worsening equity market-wide liquidity.

Third, we use the value funding liquidity proposed by Fontaine and Garcia (2012, FG), and filtered from on- and off-the-run Treasury bonds. An increase in the value of funding liquidity is interpreted as a tightening of funding conditions.

Our fourth measure, labeled "Fails," is the total monthly par value of transaction (in logarithm) that involve failures to deliver a Treasury bond needed to settled a trade.[21] In periods of a large demand for liquid collateral, market participants may choose to fail to deliver on their repo transaction.[22] As increase in the volume of fails should then be

[21] The data on fails is available from the website of the New York Fed. Alternatively, we could use the variation in haircuts applied to Treasury collateral to study the collateral channel—an increase in Treasury volatility lead to an increase in haircuts applied to Treasury collateral which trigger margin calls and thus decrease the liquidity in the market. Due to the lack of data on haircuts we analyze only the failures to deliver.

[22] Because the penalty for the failure is linked to the short term interest rate, such a situation occurs especially when the interest rates are low. Since May 2009, when a special charge for the failure was

informative about the demand pressure in the Treasury market, and the value of liquid collateral.

Finally, as a fifth variable, we consider the TED spread, i.e. the spread between the three-month LIBOR and the three-month T-bill rate. An increase in the spread is interpreted as a sign of rising credit risk in the banking system and thus tightening of credit provision to the economy.

Panel A of Table 5 presents contemporaneous regressions of each of the above liquidity proxies on the three volatility states obtained from the model. Endogeneity is a usual worry in such regression, so our results are merely a statement about the strength and direction of various correlations. We run regressions in levels and in monthly changes. For easy comparison of the coefficients all left- and right-hand side variables are standardized. The regressions reveal a significant link between interest rate volatility and liquidity. While each of the model-implied volatility states differs in terms of economic interpretation and macro variables with which it correlates, liquidity is significantly related to all of them. In general, an increasing yield volatility is associated with deteriorating liquidity conditions. The liquidity measures differ in the strength with which they load on the long- versus short-end volatility and the covariance state. With the exception of the FG factor, the financial crisis is an important event that strengthens the liquidity-volatility link, but this link also exists and is economically strong in the pre-crisis period. In rows labeled "$\bar{R}^2$ (92-07)," we report the $\bar{R}^2$ for the sample ending in December 2007.

We find that the three volatility states capture about 10% of variation in the monthly changes of HPW noise illiquidity. This relationship is stronger than the one found by Hu, Pan, and Wang (2012) for reasons that can be explained with the way we construct the volatility states: First, our volatility factors summarize content of derivatives and the realized variances obtained from high frequency data; second, they aggregate volatility information across different bond maturities.[23] Interestingly, we find a pronounced negative relationship between changes in the short-end yield volatility and the PS factor: A deteriorating equity market liquidity is associated with a simultaneous rise in the volatility of short rate expectations (t-statistics of -6.35). Before the crisis we observe a strong negative contemporaneous link between the level of the FG factor and yield volatility: To the extent

introduced, failures to deliver decreased to extremely low levels. See Garbade, Keane, Logan, Stokes, and Wolgemuth (2010) for more details.

[23]Hu, Pan, and Wang (2012) measure interest rate volatility as the return volatility of a five year bond computed with the 21 rolling window. They find a positive but insignificant relationship between monthly changes in volatility and monthly changes noise illiquidity with $\bar{R}^2$ of below 2%.

that the value of funding liquidity comoves with the actions of the Fed (empirically the FG factor decreases during easings when volatility is high), the negative sign is intuitive. The inclusion of the crisis years weakens this connection. Both the volume of fails and the TED spread increase together with yield volatility.

In panel B we study leads and lags between long- and short-end volatility factors and three liquidity measures: PS, HPW and FG. Panel B1 shows regressions when volatility is predicted with lagged liquidity, panel B2 considers the opposite case. Leads and lags are from one through 18 months. To be concise, we only report the coefficients, t-statistics and $\bar{R}^2$ for the lead/lag with the highest $\bar{R}^2$. The general conclusion from the table is that liquidity conditions forecast the long-end volatility at horizons above six months. The PS liquidity is significant at a lag of about one year with a negative sign, suggesting that a worsening liquidity in the equities market today forecasts a higher risk premium volatility of Treasuries in the future. Even though predictive regressions do not justify causal statements, this correlation would be consistent with a story in which the Fed supports the equity market through easier monetary policy trading off a higher risk of long-term Treasuries in the future. Similarly, the HPW factor predicts long-end volatility (with a positive and highly significant coefficient) at horizon of about six months. At the same time, the forecasting power of liquidity for the short-end volatility is much weaker. Rather, increasingly volatile short rate expectations anticipate declining liquidity conditions at horizons of about half a year; but the short-end volatility itself does not appear easy to forecast with lags of the liquidity proxies beyond horizons of one or two months.

V. Conclusions

We study the properties and the information contained in the volatility of the US Treasury market. We propose a flexible no-arbitrage term structure model that allows for a stochastic covariance between risk factors in the yield curve, and combine it with an estimation using nominal yields, their realized covariance matrix and interest rate derivatives. The model serves to decompose interest rate volatility into short rate expectations volatility and the volatility of the term premia, respectively, as well as their conditional covariance. We show how these components contribute to interest rate volatility across the term structure. At short maturities, interest rate volatility is mainly driven by volatile short rate expectations, but as the maturity increases the term premium volatility becomes more pronounced. Interest rate volatility factors feature distinct dynamics over the business

cycle, and contain additional information about the economy over and above the standard yield curve factors. We find that the volatility of short rate expectations predicts economic activity independently of the term spread. In particular, short rate expectations become more volatile before recessions and during times of distress in asset markets, whereas volatility of the term premia rises at the exit from a recession. Our interpretation of the volatility factors finds support with evidence from survey data and with measures of monetary and economic policy uncertainty. Studying links between interest rate volatility and liquidity, we document that risk premia in Treasuries become more volatile following periods of deteriorating liquidity in equity and bond markets.

References

Adrian, T., and H. Wu (2009): "The Term Structure of Inflation Expectations," Working Paper, Federal Reserve Bank of New York.

Andersen, T. G., and L. Benzoni (2010): "Do Bonds Span Volatility Risk in the US Treasury Market? A Specification Test for Affine Term Structure Models," *Journal of Finance*, 65, 603–655.

Andersen, T. G., T. Bollerslev, F. X. Diebold, and C. Vega (2007): "Real-Time Price Discovery in Global Stock, Bond and Foreign Exchange Markets," *Journal of International Economics*, 73, 251–277.

Ang, A., J. Boivin, S. Dong, and R. Loo-Kung (2010): "Monetary Policy Shifts and the Term Structure," *Review of Economic Studies*, forthcoming.

Baker, S. R., N. Bloom, and S. J. Davis (2013): "Measuring Economic Policy Uncertainty," Working paper, Stanford University and University of Chicago.

Barndorff-Nielsen, O. E., and N. Shephard (2004): "Econometric Analysis of Realised Covariation: High Frequency Based Covariance, Regression and Correlation in Financial Economics," *Econometrica*, 72, 885–925.

Bekker, P. A., and K. E. Bouwman (2009): "Risk-free Interest Rates Driven by Capital Market Returns," Working paper, University of Groningen and Erasmus University Rotterdam.

Bru, M.-F. (1991): "Wishart Processes," *Journal of Theoretical Probability*, 4, 725–751.

Campbell, J. Y., A. Sunderam, and L. M. Viceira (2013): "Inflation Bets or Deflation Hedges? The Changing Risk of Nominal Bonds," Working paper, Harvard Business School.

Carr, P., and L. Wu (2006): "A Tale of Two Indices," *Journal of Derivatives*, pp. 13–29.

——— (2007): "Stochastic Skew in Currency Options," *Journal of Financial Economics*, 86, 213–247.

Chan, K. C., G. A. Karolyi, F. A. Longstaff, and A. B. Sanders (1992): "An Empirical Comparison of Alternative Models of the Short-Term Interest Rate," *Journal of Finance*, 47, 1209–1227.

Christoffersen, P., K. Jacobs, L. Karoui, and K. Mimouni (2009): "Non-Linear Filtering in Affine Term Structure Models: Evidence from the Term Structure of Swap Rates," Working paper, University of Toronto Rotman School of Management.

Cochrane, J. H., and M. Piazzesi (2005): "Bond Risk Premia," *American Economic Review*, 95, 138–160.

Collin-Dufresne, P., and R. S. Goldstein (2002): "Do Bonds Span the Fixed Income Markets? Theory and Evidence for the Unspanned Stochastic Volatility," *Journal of Finance*, 58, 1685–1730.

Collin-Dufresne, P., R. S. Goldstein, and C. S. Jones (2009): "Can Interest Rate Volatility Be Extracted from the Cross-Section of Bond Yields?," *Journal of Financial Economics*, 94, 47–66.

Cox, J. C., J. E. Ingersoll, and S. A. Ross (1985): "A Theory of the Term Structure of Interest Rates," *Econometrica*, 53, 373–384.

Dai, Q., and K. Singleton (2000): "Specification Analysis of Affine Term Structure Models," *Journal of Finance*, 55, 1943–1978.

Diether, K., C. Malloy, and A. Scherbina (2002): "Differences in Opinion and the Cross-Section of Stock Returns," *Journal of Finance*, 57, p. 2113 – 2141.

Duffee, G. R. (2002): "Term Premia and Interest Rate Forecasts in Affine Models," *Journal of Finance*, 57, 405–443.

——— (2011): "Information in (and Not in) the Term Structure," *Review of Financial Studies*, 24, 2895–2934.

Estrella, A., and G. A. Hardouvelis (1991): "The Term Structure as a Predictor of Real Economic Activity," *Journal of Finance*, 46, 555–576.

Fisher, M., D. Nychka, and D. Zervos (1994): "Fitting the Term Structure of Interest Rates with Smoothing Splines," Working paper, Federal Reserve and North Carolina State University.

Fleming, M. J. (1997): "The Round-the-Clock Market for U.S. Treasury Securities," *FRBNY Economic Policy Review*.

Fleming, M. J., and B. Mizrach (2009): "The Microstructure of a U.S. Treasury ECN: The BrokerTec Platform," Working paper, Federal Reserve Bank of New York and Rutgers University.

Fontaine, J.-S., and R. Garcia (2012): "Bond Liquidity Premia," *Review of Financial Studies*, 25, 1207–1254.

Garbade, K., F. Keane, L. Logan, A. Stokes, and J. Wolgemuth (2010): "The Introduction of the TMPG Fails Charge for U.S. Treasury Securities," *FRBNY Economic Policy Review*, pp. 45–71.

Gourieroux, C. (2006): "Continuous Time Wishart Process for Stochastic Risk," *Econometric Reviews*, 25, 177–217.

Gourieroux, C., J. Jasiak, and R. Sufana (2009): "The Wishart Autoregressive Process of Multivariate Stochastic Volatility," *Journal of Econometrics*, 150, 167–181.

Harvey, C. R. (1989): "Forecasts of Economic Growth from the Bond and Stock Markets," *Financial Analysts Journal*, September–October, 38–45.

Haubrich, J., G. Pennacchi, and P. Ritchken (2012): "Inflation Expectations, Real Rates, and Risk Premia: Evidence from Inflation Swaps," *Review of Financial Studies*, 25, 1588–1629.

Hautsch, N., and Y. Ou (2008): "Yield Curve Factors, Term Structure Volatility, and Bond Risk Premia," Working paper, Humboldt Univeristy Berlin.

Hayashi, T., and N. Yoshida (2005): "On covariance estimation of non-synchronously observed diffusion processes," *Bernoulli*, 11, 359–379.

Heidari, M., and L. Wu (2003): "Are Interest Rate Derivatives Spanned by the Term Structure of Interest Rates?," *Journal of Fixed Income*, 13, 75–86.

Hu, X., J. Pan, and J. Wang (2012): "Noise as Information for Illiquidity," *Journal of Finance,* forthcoming.

Jacobs, K., and L. Karoui (2009): "Conditional Volatility in Affine Term-Structure Models: Evidence from Treasury and Swap Markets," *Journal of Financial Economics*, 91, 288–318.

Jacod, J. (1994): "Limit of Random Measures Associated with the Increments of a Brownian Semimartingale," Working paper, Universite Pierre et Marie Curie.

Jones, C. M., O. Lamont, and R. L. Lumsdaine (1998): "Macroeconomic News and Bond Market Volatility," *Journal of Financial Economics*, 47, 315–337.

Joslin, S. (2007): "Pricing and Hedging Volatility Risk in Fixed Income Markets," Working paper, USC Marshall.

JP Morgan (2011): "The Domino Effect of a US Treasury Technical Default," *US Fixed Income Strategy*, April 19, 2011.

Julier, S., and J. Uhlmann (1997): "A new extension of the Kalman filter to nonlinear systems," *in Proceedings of AeroSense: The 11th International Symposium on Aerospace/Defence Sensing, Simulation and Controls*.

Kim, D. H., and K. J. Singleton (2012): "Term Structure Models and the Zero Bound: An Empirical Investigation of Japanese Yields," *Journal of Econometrics*, 170, 32–49, Working Paper, Yonsei University and Stanford University.

Krishnamurthy, A., and A. Vissing-Jorgensen (2010): "The Aggregate Demand for Treasury Debt," *Journal of Political Economy*, 120, 233–267.

Li, H., and F. Zhao (2006): "Unspanned Stochastic Volatility: Evidence from Hedging Interest Rate Derivatives," *Journal of Finance*, 61, 341–378.

Longstaff, F. (2004): "The Flight to Liquidity Premium in U.S. Treasury Bond Prices," *Journal of Business*, 77, 511–526.

Mizrach, B., and C. J. Neely (2006): "The Transition to Electronic Communications Networks in the Secondary Treasury Market," *Federal Reserve Bank of St. Louis Review*.

Pastor, L., and R. Stambaugh (2003): "Liquidity Risk and Expected Stock Returns," *Journal of Political Economy*, 111, 642–685.

Phoa, W. (1997): "Can You Derive Market Volatility Forecast from the Observed Yield Curve Convexity Bias?," *Journal of Fixed Income*, pp. 43–53.

Price, K. V., R. M. Storn, and J. A. Lampinen (2005): *Differential Evolution: A Practical Approach to Global Optimization*. Springer Berlin.

SIFMA (2010): "Research Quarterly, Third Quarter 2010," http://www.sifma.org/research/item.aspx?id=2234.

Thornton, D. (2012): "Greenspan's Conundrum and the Fed's Ability to Affect Long Term Yields," Working paper, St. Louis Fed.

Vayanos, D., and P.-O. Weil (2008): "A Search-Based Theory of the On-the-Run Phenomenon," *Journal of Finance*, 63, 1361–1398.

Appendix A. Figures

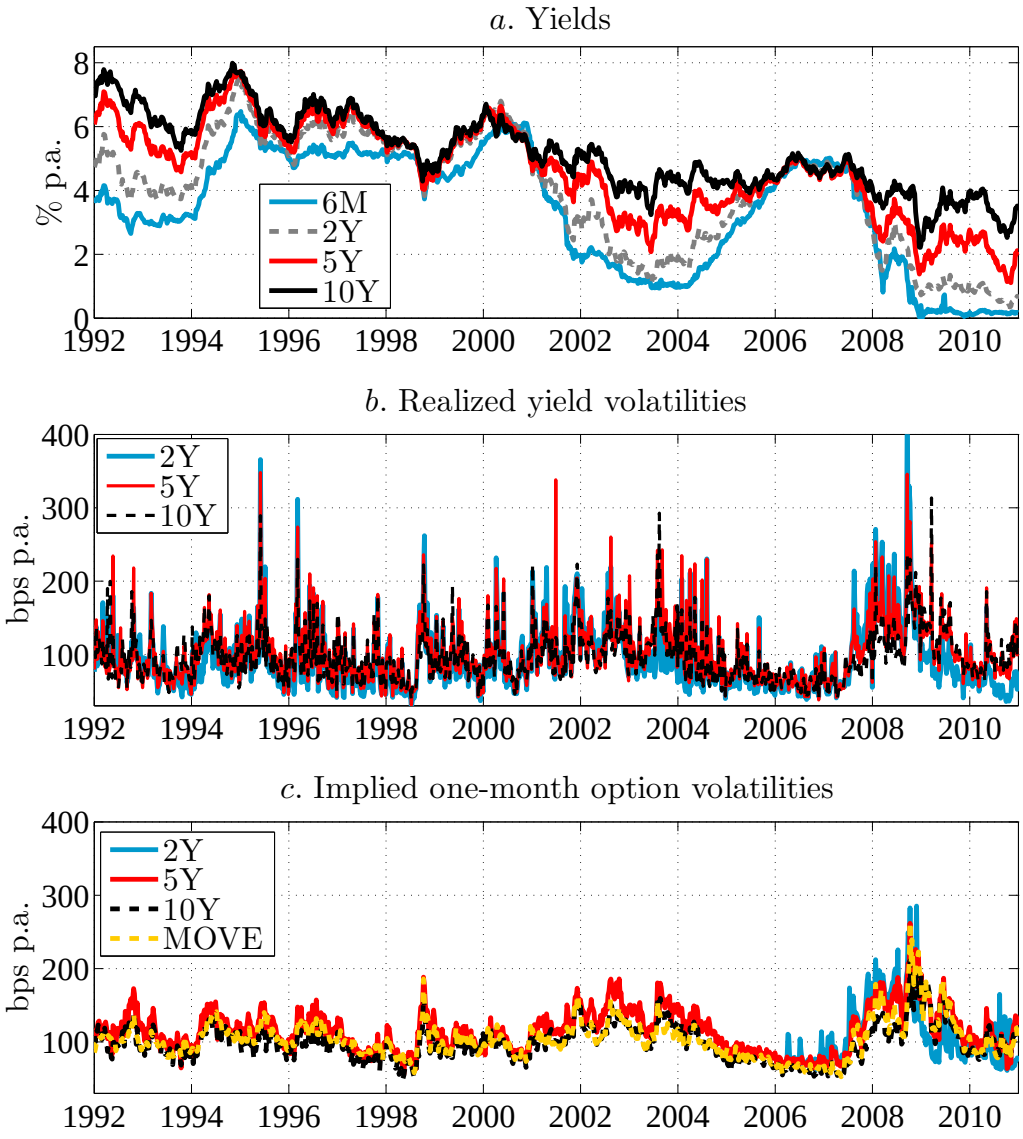

Figure 1: Time series of yields and volatilities

The figure plots the time series of yields, realized volatilities and implied volatilities over the 1992:01–2010:12 sample. The data are sampled weekly. Yields include maturities of six months and two, five, and ten years (panel *a*). Realized volatilities are constructed for bonds with two, five and ten years to maturity (panel *b*). Implied volatilities are constructed for the two-, five- and ten-year bond; the implied volatility series for the two-year note starts in March 2006 (panel *c*). We additionally superimpose the implied volatilities with the MOVE index which is a weighted average of yield volatilities for maturities up to 30-years.

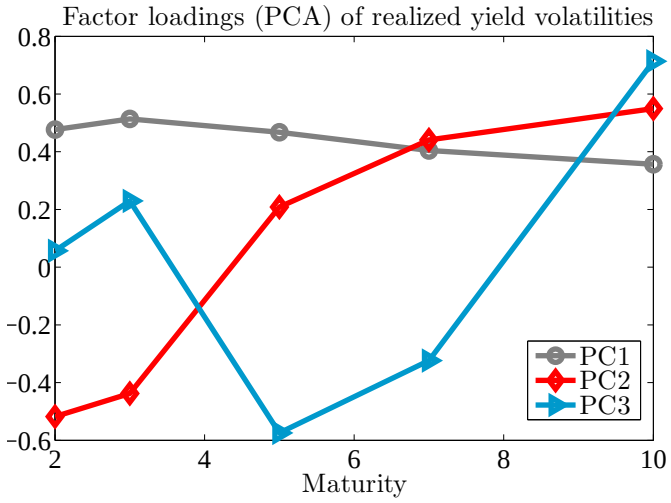

Figure 2: Factors in yield volatilities

The figure shows the principal component decomposition of the realized yield volatilities. We use the unconditional correlation matrix of realized weekly volatilities computed for two-, three-, five-, seven- and ten-year zero-coupon bonds.

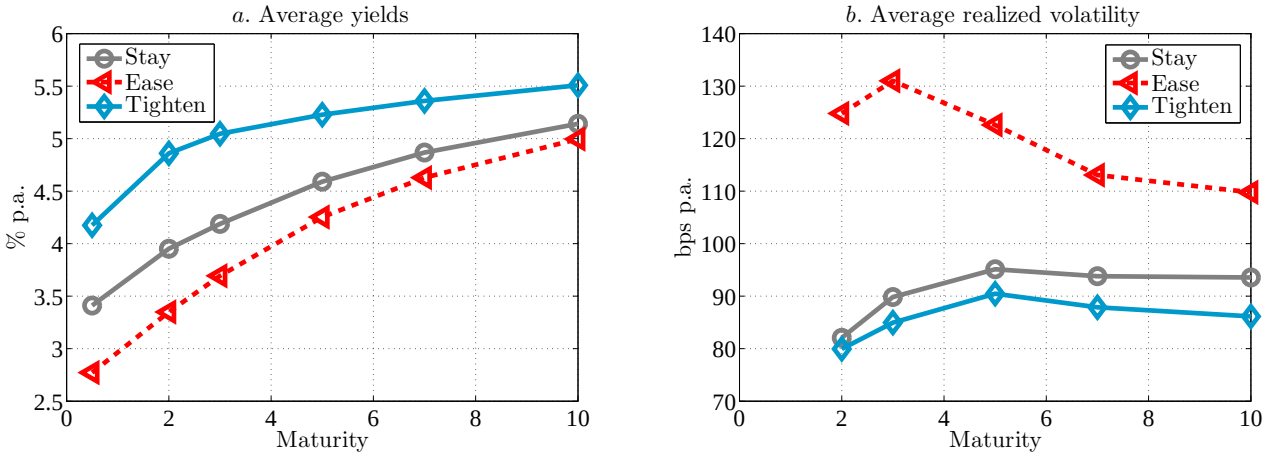

Figure 3: Yield and volatility curves

The figure plots the unconditional means of yields and volatilities for different maturities. It reports the unconditional means for the whole sample 1992:01–2010:12, and means conditional on the Fed's tightening and easing cycles, or no action (denoted as "stay" in the graph). A period is classified as easing, tightening or stay if it spans at least three subsequent moves in the federal funds rate target in a respective direction. The realized volatility curves are computed from the weekly data and annualized.

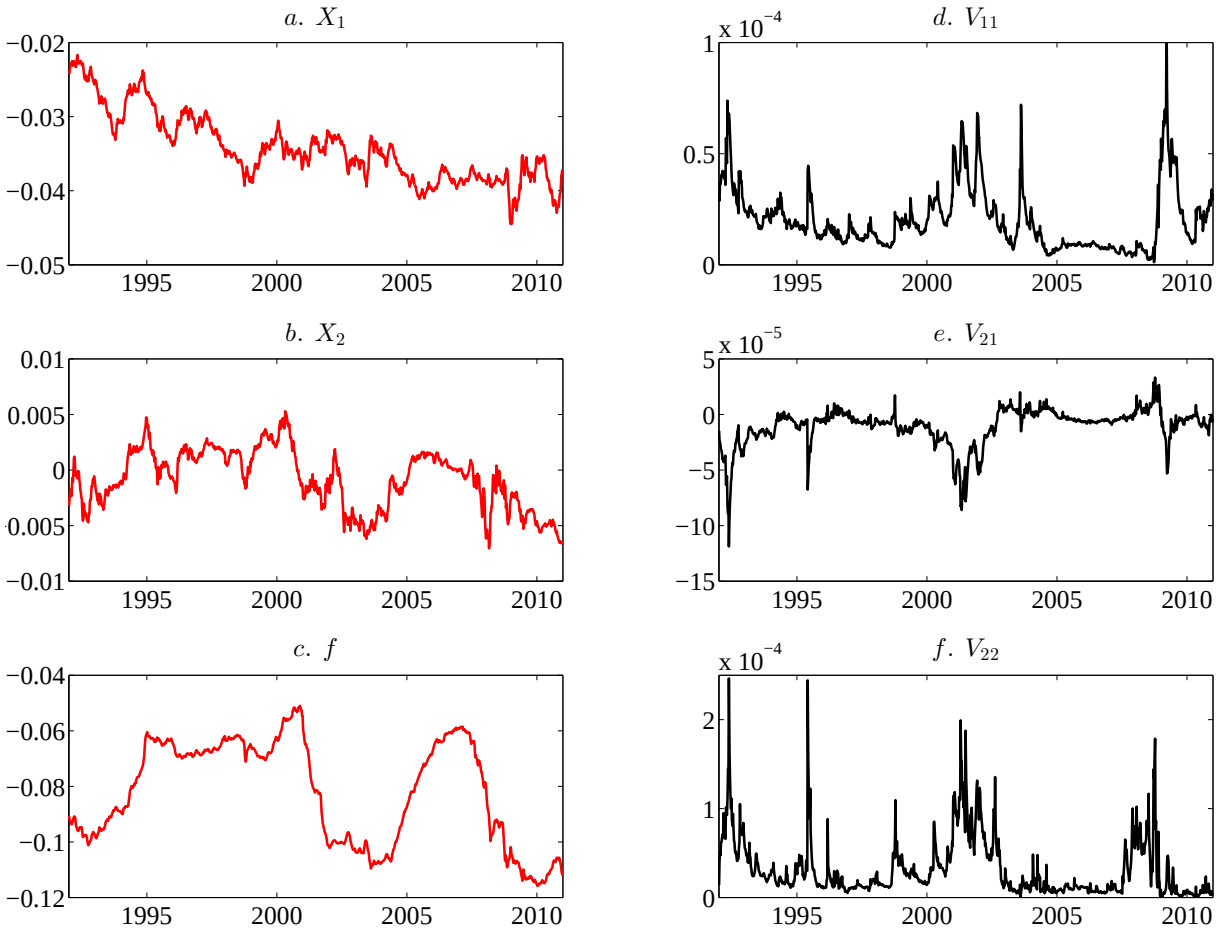

Figure 4: Model-implied factor dynamics

The figure plots the model-implied factor dynamics. The left-hand panels present factors driving the yield curve. The right-hand panels display factors driving the conditional second moments of yields. The sample period is 1992:01–2010:12 with weekly sampling.

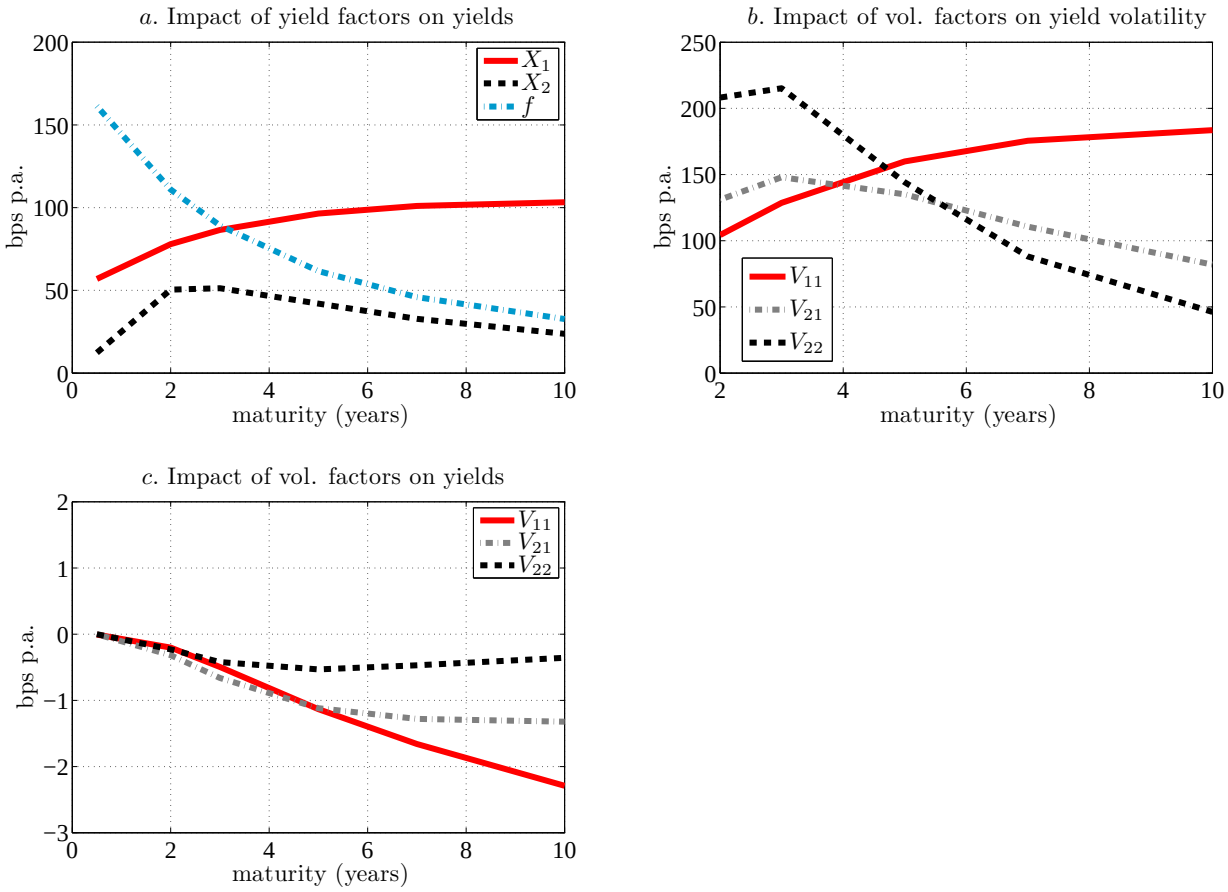

Figure 5: Impact of yield and volatility factors on the yield curve

Panel *a* plots the impact of one standard deviation shock to the yield curve factors on the yield curve. Panel *b* shows the impact of one standard deviation shock to volatility factors on yield volatilities at different maturities. Panel *c* displays the impact of volatility factors on the yield curve.

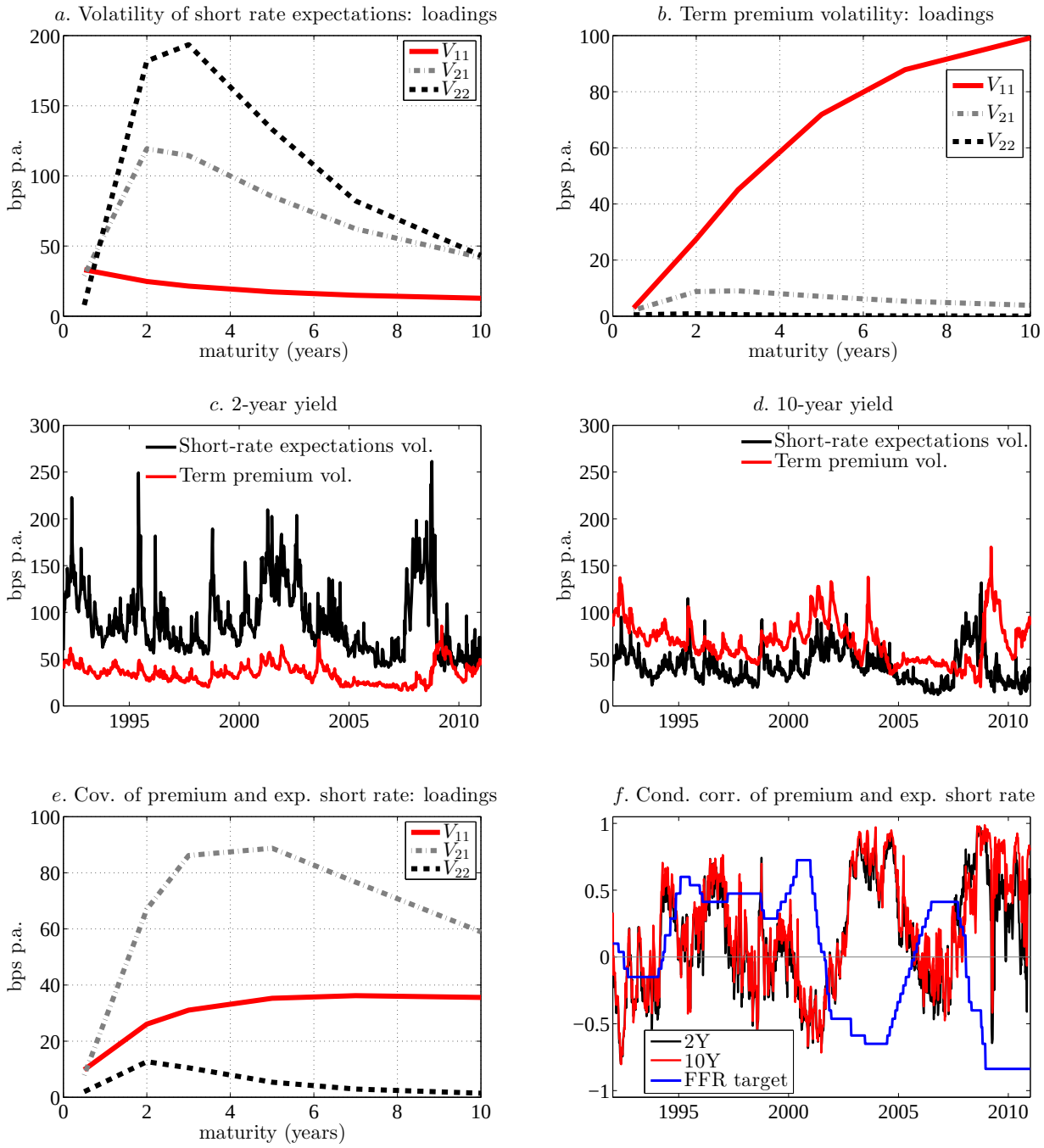

Figure 6: Volatility of short-rate expectations and risk premium

The figure plots the model-based decomposition of yield volatility into short-rate expectations volatility and the risk premium volatility, as well as the conditional covariance between expectations and premia. Panels *a*, *b* and *e* show how each volatility factor from the model contributes to the respective volatilities and to the covariance. All loadings are reported per square root of a unit standard deviation in the corresponding factor and converted into basis points. Panels *c* and *d* present the time series of the respective volatility components for the two- and the ten-year yield. Panel *f* shows the conditional correlation between the term premia and short rate expectations for the two- and the ten-year maturity. The blue step line in panel *f* superimposes the (rescaled) FFR target.

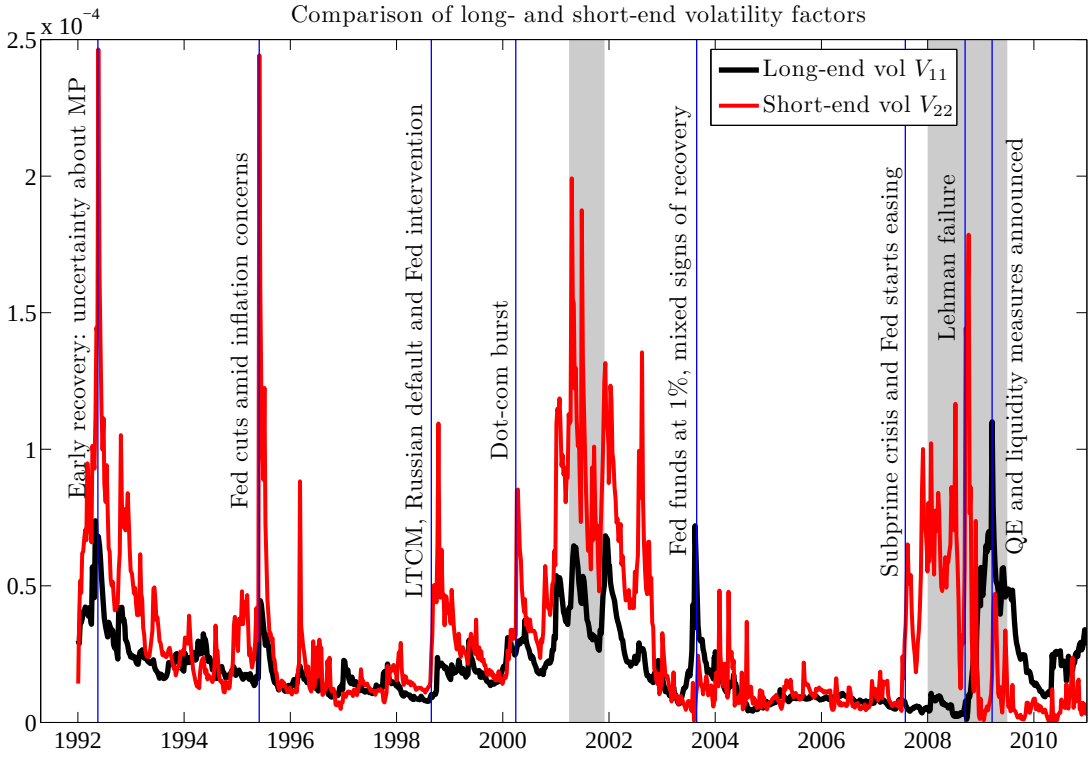

Figure 7: Short- and long-end volatility factors and selected events

The figure plots the model-implied dynamics for the long-end (V_{11}) and the short-end volatility (V_{22}) states. Shaded areas are the NBER-dated recessions. Vertical lines mark major economic or financial events.

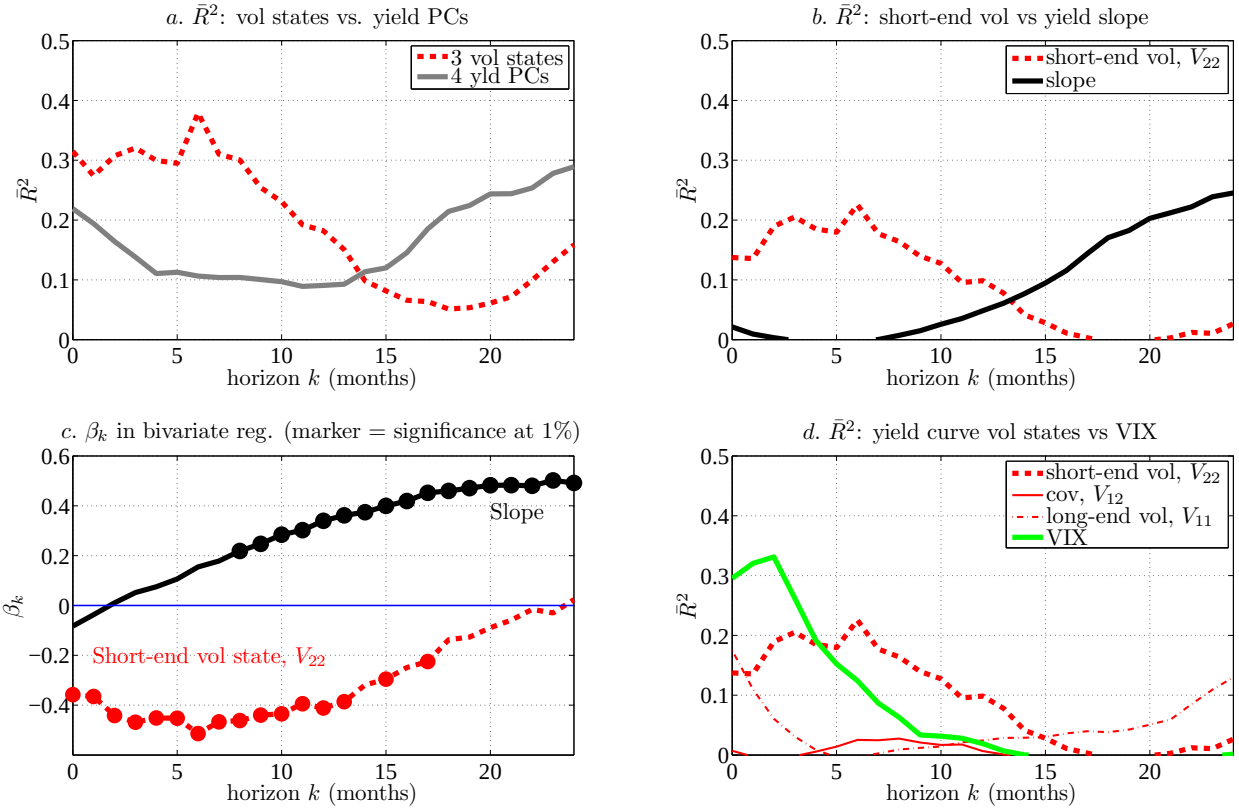

Figure 8: Predicting economic activity with the yield curve information

The figure presents results of predictive regressions of the Chicago Fed National Activity Index (CFNAI) on the yield curve and yield volatility states. The regression is

$$\text{CFNAI}_{t+k} = \beta_0 + \beta_k' X_t + \varepsilon_{t+k}$$

where X_t is a given regressor or a vector of regressors, k is horizon in months (between 0 and 24). In panel a, we report the $\bar{R}^2$s from two regressions: (i) using three volatility states obtained from the model and (ii) using the first four PCs extracted from the yield curve. In panel b, we run univariate predictive regressions with the short-end volatility state V_{22} and the term structure slope as explanatory variables, respectively. In panel c, we report the standardized beta coefficients β_k from bivariate predictive regressions using slope and the short-end volatility jointly. Markers (circles) indicate cases in which the regression coefficient is significant at the 1% level. Panel d displays the $\bar{R}^2$s from univariate regressions run separately on each yield volatility state, and on the VIX. The data are at the monthly frequency, and the sample period is 1992:01–2010:12.

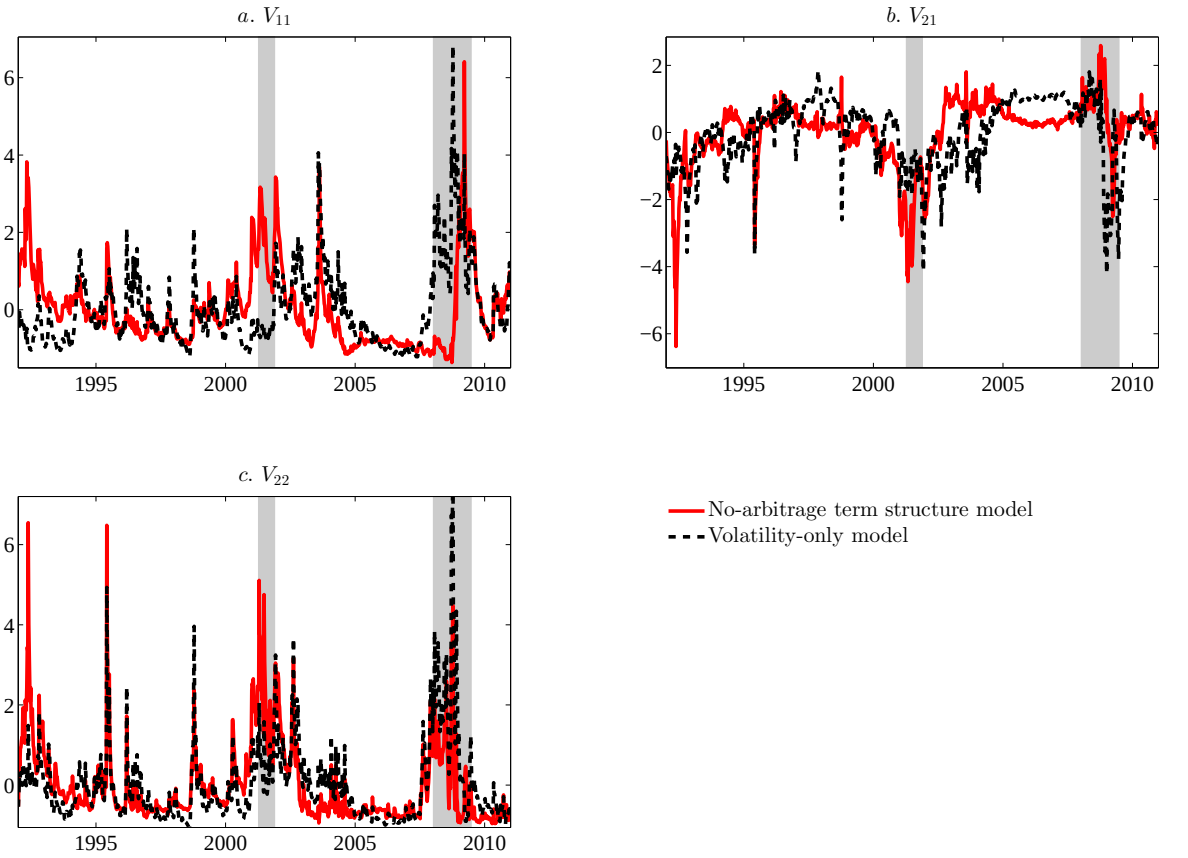

Figure 9: Volatility-only versus no-arbitrage term structure model

The figure compares filtered volatility factors from the no-arbitrage term structure model with the factors from the volatility-only model. Both models are estimated using identical volatility measurements. Shaded areas mark the NBER-dated recessions. The sample period is 1992:01–2010:12 with weekly sampling. All factors are standardized.

Appendix B. Tables

Table 1: Descriptive statistics of weekly yields and realized volatilities

The table contains descriptive statistics of weekly yields (panel A) and realized yield volatilities (panel B). Implied volatilities statistics in panel B are for coupon bonds, which is marked with the superscript "(c)" in the column heading. Panel C shows unconditional correlations between yields, realized volatilities, and implied volatilities, as well as with the Merrill Option Implied Volatility (MOVE) index. The sample period is 1992:01–2010:12, except for the implied volatility on a two-year bond (marked with $\star$), for which the data begins in March 2006. AR(1m) denotes the autoregressive coefficient estimated for overlapping monthly data sampled at the weekly frequency.

A. Yields (% p.a.)

	6M	2Y	3Y	5Y	7Y	10Y
Mean	3.39	3.97	4.23	4.63	4.90	5.18
Skew	-0.39	-0.37	-0.36	-0.25	-0.09	0.13
Kurt	1.84	2.00	2.11	2.20	2.24	2.28
AR(1m)	0.998	0.995	0.992	0.985	0.980	0.975

B. Volatilities (bps p.a.)

	2Y	3Y	5Y	7Y	10Y
Realized volatilities					
Mean	93.19	99.98	101.61	97.81	96.44
Stdev	43.63	46.29	41.41	36.95	34.59
Skew	2.08	2.07	1.65	1.35	1.53
Kurt	10.89	10.45	7.61	5.80	7.31
AR(1m)	0.44	0.39	0.41	0.44	0.42
Implied volatilities	$2Y^{\star(c)}$		$5Y^{(c)}$		$10Y^{(c)}$
Mean	112.71		115.39		98.72
Stdev	45.04		29.43		24.55
Skew	1.13		0.64		0.69
Kurt	3.79		3.58		4.05
AR(1m)	0.71		0.81		0.83

C. Unconditional correlations of yields, realized volatilities, and implied volatilities

	y_t^{6M}	y_t^{2Y}	y_t^{3Y}	y_t^{5Y}	y_t^{7Y}	y_t^{10Y}	RVol_t^{2Y}	RVol_t^{3Y}	RVol_t^{5Y}	RVol_t^{7Y}	RVol_t^{10Y}
y_t^{6M}	1.00	·	·	·	·	·	·	·	·	·	·
y_t^{2Y}	0.97	1.00	·	·	·	·	·	·	·	·	·
y_t^{3Y}	0.95	0.99	1.00	·	·	·	·	·	·	·	·
y_t^{5Y}	0.88	0.96	0.98	1.00	·	·	·	·	·	·	·
y_t^{7Y}	0.81	0.91	0.95	0.99	1.00	·	·	·	·	·	·
y_t^{10Y}	0.74	0.85	0.90	0.96	0.99	1.00	·	·	·	·	·
RVol_t^{2Y}	-0.13	-0.12	-0.10	-0.08	-0.06	-0.04	1.00	·	·	·	·
RVol_t^{3Y}	-0.18	-0.15	-0.12	-0.09	-0.06	-0.02	0.95	1.00	·	·	·
RVol_t^{5Y}	-0.27	-0.24	-0.22	-0.20	-0.17	-0.13	0.89	0.90	1.00	·	·
RVol_t^{7Y}	-0.33	-0.30	-0.28	-0.24	-0.21	-0.17	0.81	0.85	0.97	1.00	·
RVol_t^{10Y}	-0.32	-0.27	-0.25	-0.21	-0.17	-0.13	0.75	0.78	0.89	0.93	1.00

Unconditional correlations of implied and realized yield volatilities

	RVol_t^{2Y}	RVol_t^{3Y}	RVol_t^{5Y}	RVol_t^{7Y}	RVol_t^{10Y}	$\text{IV}^{2Y\star}$	IV^{5Y}	IV^{10Y}	MOVE
$\text{IV}^{2Y\star}$	0.80	0.75	0.70	0.60	0.53	1.00	·	·	·
IV^{5Y}	0.62	0.61	0.65	0.66	0.63	0.79	1.00	·	·
IV^{10Y}	0.51	0.52	0.61	0.65	0.66	0.59	0.94	1.00	·
MOVE	0.61	0.60	0.67	0.69	0.68	0.71	0.91	0.91	1.00

Table 2: Model-implied expected bond returns

The table reports the regression results for realized annual bond excess returns with maturities 2, 3, 5, 7 and 10 years on the corresponding model-implied expected returns (panel A), on the Gaussian part of the model-implied returns (panel B) and on the Cochrane-Piazzesi factor (panel C). The row "p-val $\beta = 1$" tests the restriction that the regression coefficient is equal to one. Rows "AR(1m)" report the monthly AR(1) coefficient for realized and model-implied expected excess returns. Panels D and E report the regression results for monthly non-overlapping bond excess returns (CRSP portfolios) on model-implied instantaneous expected excess returns. The monthly frequency of data in panels D and E is dictated by the availability of the CRSP realized bond returns. The data span the period 1992:01–2010:12. T-statistics in parentheses are Newey-West adjusted with 18 lags.

	rx_2	rx_3	rx_5	rx_7	rx_{10}
A. Annual model-implied expected returns					
α	0.00	0.01	0.02	0.02	0.03
	(1.08)	(1.70)	(2.60)	(2.87)	(2.80)
β	0.76	0.98	1.63	2.46	3.79
	(1.74)	(1.77)	(2.18)	(2.74)	(3.41)
R^2	0.03	0.04	0.06	0.09	0.13
p-val $\beta = 1$	0.58	0.97	0.40	0.10	0.01
AC(1m) realized ret.	0.95	0.94	0.92	0.90	0.88
AC(1m) model-implied ret.	0.96	0.96	0.96	0.96	0.95
B. Annual model-implied expected returns (Gaussian part)					
α	0.01	0.01	0.02	0.02	-0.02
	(1.94)	(2.30)	(2.16)	(1.07)	(-0.79)
β	0.77	1.01	1.69	2.59	4.06
	(1.28)	(1.33)	(1.70)	(2.21)	(2.99)
R^2	0.04	0.04	0.06	0.10	0.15
C. Annual expected returns: Cochrane-Piazzesi factor					
α	0.00	0.01	0.01	0.01	0.01
	(1.06)	(0.93)	(0.86)	(0.82)	(0.74)
β	1.12	2.40	4.87	7.10	9.87
	(1.82)	(1.98)	(2.31)	(2.66)	(3.11)
R^2	0.08	0.10	0.14	0.17	0.19
D. Monthly model-implied expected returns (CRSP portfolios)					
	$rx < 24m$	$rx < 36m$	$rx < 48m$	$rx < 60m$	$rx < 120$
α	0.04	0.04	0.04	0.03	-0.01
	(5.43)	(5.10)	(3.62)	(2.40)	(-0.20)
β	1.74	1.77	2.01	2.32	2.83
	(2.86)	(2.42)	(2.45)	(2.44)	(2.70)
R^2	0.06	0.03	0.02	0.02	0.02
E. Monthly model-implied expected returns (Gaussian part, CRSP portfolios)					
α	0.04	0.04	0.03	0.03	-0.02
	(5.19)	(4.53)	(2.64)	(1.52)	(-0.71)
β	1.73	1.73	1.93	2.21	2.77
	(2.82)	(2.34)	(2.34)	(2.33)	(2.75)
R^2	0.06	0.03	0.02	0.02	0.02

Table 3: Correlations of volatility factors

This table reports unconditional correlations of model-based volatility factors and principal components obtained from realized and implied volatilities. "V_{ii}^{NA}" denotes our baseline no-arbitrage model, "V_{11}^{SV}" denotes the volatility-only model and "PCi" is the i-th principal component. The sample period is 1992:01–2010:12.

	V_{11}^{NA}	V_{21}^{NA}	V_{22}^{NA}	V_{11}^{SV}	V_{21}^{SV}	V_{22}^{SV}	PC1	PC2	PC3
V_{11}^{NA}	1.00	.	.	.	.	.	.	.	.
V_{21}^{NA}	-0.72	1.00	.	.	.	.	.	.	.
V_{22}^{NA}	0.48	-0.68	1.00	.	.	.	.	.	.
V_{11}^{SV}	0.28	0.32	0.16	1.00	.	.	.	.	.
V_{21}^{SV}	-0.77	0.40	-0.44	-0.38	1.00	.	.	.	.
V_{22}^{SV}	0.19	-0.01	0.70	0.70	-0.41	1.00	.	.	.
PC1	0.27	0.05	0.55	0.72	-0.42	0.84	1.00	.	.
PC2	-0.38	-0.14	0.12	-0.54	0.54	-0.18	0.00	1.00	.
PC3	0.29	-0.08	-0.27	-0.03	-0.08	-0.38	0.00	0.00	1.00

Table 4: Regressions of filtered states on macroeconomic surveys

This table reports regressions of the model-implied volatility factors on macroeconomic surveys. Monthly factors are obtained by averaging the weekly numbers returned from the estimation within a given month. Survey data are from the Blue Chip Financial Forecasts. Forecasters predict the real GDP (RGDP), the federal funds rate (FFR), and the consumer price index (CPI) at horizons from the current through four quarters ahead. $dE(\cdot)$ denotes the change in the consensus forecast from one month to the next, where the consensus is defined as a median forecast (averaged across forecast horizons); $\sigma(\cdot)$ proxies for the uncertainty, and is computed as the mean absolute deviation of individual forecasts (also averaged across forecast horizons). σPOL is the economic policy uncertainty index from Baker, Bloom, and Davis (2013). T-statistics are corrected using Newey-West adjustment with 12 lags and are reported in parentheses. For ease of comparison, both the left and right hand side variables are standardized.

	A. Sample including crisis, 1992-2010			B. Sample excluding crisis, 1992-2006		
	Long-end V_{11}	Cov V_{21}	Short-end V_{22}	Long-end V_{11}	Cov V_{21}	Short-end V_{22}
dE(CPI)	0.02	-0.03	-0.06	0.01	0.01	0.04
	(0.43)	(-0.70)	(-0.90)	(0.26)	(0.36)	(1.28)
dE(FFR)	0.09	-0.02	-0.25	0.14	0.05	-0.22
	(1.30)	(-0.23)	(-3.49)	(2.23)	(0.62)	(-3.34)
dE(RGDP)	0.24	-0.16	0.02	0.15	-0.05	0.05
	(6.50)	(-2.99)	(0.52)	(2.81)	(-0.75)	(0.71)
σ(CPI)	-0.10	0.38	-0.07	-0.18	0.09	0.05
	(-0.73)	(2.63)	(-0.63)	(-2.82)	(1.03)	(0.77)
σ(FFR)	-0.08	0.14	0.32	0.09	-0.04	0.29
	(-0.63)	(0.99)	(2.63)	(0.77)	(-0.25)	(2.41)
σ(RGDP)	0.32	-0.29	0.38	0.35	-0.31	0.34
	(2.88)	(-1.81)	(3.53)	(3.18)	(-2.34)	(3.06)
σ(POL)	0.43	-0.19	0.05	0.33	0.00	0.15
	(3.52)	(-1.61)	(0.57)	(3.59)	(-0.01)	(1.20)
$\bar{R}^2$	0.42	0.14	0.38	0.36	0.09	0.43

Table 5: Liquidity measures and yield volatility

Panel A summarizes contemporaneous regressions of liquidity measures on the model-based volatility factors. HPW is the noise illiquidity of Hu, Pan, and Wang (2012) obtained from Treasuries; PS is the equity market-wide liquidity measures of Pastor and Stambaugh (2003); FG is the Fontaine and Garcia (2012) funding liquidity from the Treasuries; Fails are the par value of transactions (in logs) in Treasuries that have failed to be delivered. TED is the spread between the three-month LIBOR and 3-month Tbill rate. In the two subpanels, the regressions are run in levels and in monthly changes, respectively. For comparison, rows denoted "$\bar{R}^2$ (92-07)" report the corresponding $\bar{R}^2$ for the sample ending in 2007:12. Panel B summarizes the lead and lag relationship between the short- and long-end volatility factors and PS, HPW and FG liquidity. Panel B1 (leads of vol) reports the results for predicting volatility with liquidity measures; Panel B2 (lags of vol) reports the results for predicting the liquidity measures with the lags of volatility. While we consider leads and lags up to 18 months, we report only results for the horizon where the predictability is the highest as measured by the $\bar{R}^2$. k is the horizon in months, β_k is the standardized regression coefficients, t(β_k) is the t-statistics, "Before crisis" summarizes whether the relationship is stronger (S) or weaker (W) or qualitatively similar (Unch) before the crisis (i.e. sample ending in 2007:12). The predictive regressions are estimated in levels. In panels A and B, the regression coefficients are standardized and t-statistics are with Newey-West adjustment with 12 lags. The data is at the monthly frequency. The sample is 1992:01–2010:12.

A. Contemporaneous regressions

	HPW	PS	FG	Fails	TED
Levels					
Long-end vol, V_{11}	0.74	-0.20	-0.02	0.42	0.04
	(2.49)	(-2.20)	(-0.08)	(2.72)	(0.15)
Cov, V_{21}	0.57	-0.37	0.10	0.55	0.50
	(2.35)	(-4.18)	(0.41)	(4.16)	(2.04)
Short-end vol, V_{22}	0.33	-0.30	-0.26	0.29	0.50
	(3.54)	(-4.87)	(-1.46)	(2.69)	(2.85)
$\bar{R}^2$	0.46	0.11	0.09	0.22	0.28
$\bar{R}^2$ (92-07)	0.26	0.08	0.38	0.10	0.20
Monthly changes					
Long-end vol, V_{11}	0.19	-0.05	-0.06	0.26	0.12
	(3.14)	(-0.75)	(-0.84)	(5.62)	(2.18)
Cov, V_{21}	0.31	-0.11	0.05	0.20	0.27
	(3.11)	(-2.52)	(0.61)	(3.23)	(3.60)
Short-end vol, V_{22}	0.16	-0.34	0.08	0.27	0.51
	(2.57)	(-6.35)	(1.37)	(3.95)	(3.09)
$\bar{R}^2$	0.09	0.10	0.00	0.11	0.26
$\bar{R}^2$ (92-07)	0.10	0.06	0.02	0.05	0.11

B. Leads and lags

	B1. Leads of vol					B2. Lags of vol				
Measure	k (m)	β_k	t(β_k)	$\bar{R}^2$	Before crisis	k (m)	β_k	t(β_k)	$\bar{R}^2$	Before crisis
Long-end vol, V_{11}										
PS	15	-0.27	-2.69	0.07	S	5	0.12	1.90	0.01	W
HPW	5	0.69	13.96	0.48	W	1	0.38	2.66	0.14	Unch
FG	1	-0.15	-0.72	0.02	S	7	-0.45	-2.85	0.20	S
Short-end vol, V_{22}										
PS	1	-0.22	-2.42	0.04	W	7	-0.16	-1.67	0.02	W
HPW	1	0.31	2.27	0.09	S	4	0.45	1.93	0.20	S
FG	2	-0.31	-1.87	0.09	S	9	-0.41	-1.89	0.17	S

Appendix for:

Information in the term structure of yield curve volatility

Anna Cieslak and Pavol Povala*

This version: September, 2013

*Cieslak is at the Northwestern University, Kellogg School of Management. Povala is at the University of London, Birkbeck. Cieslak: a-cieslak@kellogg.northwestern.edu, Department of Finance, Kellogg School of Management, Northwestern University, 2001 Sheridan Road Evanston, IL 60208, phone: +1 847 467 2149. Povala: p.povala@bbk.ac.uk, Birkbeck, University of London, Malet Street, Bloomsbury, London WC1E 7HX, UK, phone: +44 207 631 6486.

Contents

I. Data description

This section gives a brief description of the high-frequency Treasury data, our zero curve construction methodology, and macroeconomic surveys.

I.A. GovPX and BrokerTec

The US Treasury market is open around the clock, but the trading volumes and volatility are concentrated during the New York trading hours. Roughly 95% of trading occurs between 7:30AM and 5:00PM EST (see also Fleming, 1997). This interval covers all major macroeconomic and monetary policy announcements, which are commonly scheduled either for 9:00AM EST or 2:15PM EST. We consider this time span as a trading day. Around US bank holidays, there are trading days with a very low level of trading activity. In such cases, we follow the approach of Andersen and Benzoni (2010) and delete days with no trading for more than three hours.

We choose the ten-minute sampling frequency so that it strikes the balance between the non-synchronicity in trading and the efficiency of the realized volatility estimators (Zhang, Mykland, and Ait-Sahalia, 2005).

The microstructure noise does not appear to be an issue in our data, as indicated by the volatility signature plots and very low autocorrelation of equally spaced yield changes, see Figure 1.

The liquidity in the secondary bond market is concentrated in two-, three-, five- and ten-year securities (see also Fleming and Mizrach, 2009, Table 1). We assume that the dynamics of this most liquid segment spans the information content of the whole curve. Since any method for bootstrapping the zero curve is precise for maturities close to the observed yields, for subsequent covolatility analysis we select yields which are closest to the observed coupon bond maturities.

Table I reports some basic statistics on the Treasury bond transaction data in the period 1992:01 through 2010:12. For the GovPX period (1992:01–2000:12), we report the average number of quotes per trading day and for the BrokerTec period (2001:01–2010:12) we report the average number of transactions per trading day. The number of Treasury bonds and bills totals to 1148 in our sample period. These were transacted or quoted more than 49.3 million times in the on-the-run secondary market.

Table I: Average number of quotes/trades per day in the GovPX and BrokerTec databases

Bond maturity	GovPX period	BrokerTec period
3M	374	–
6M	352	–
2Y	2170	1414
3Y	1385	1017
5Y	3128	2801
7Y	637	1500
10Y	2649	2659
30Y	793	1114

I.B. Testing for microstructure noise

To avoid potential bias in the estimates of the realized volatility using high-frequency data, we apply several tests for the presence of noise caused by the market microstructure effects. In a first step, we compute the first order autocorrelation in high-frequency price returns. Table II reports the first order autocorrelation of equally-spaced ten-minute yield changes in the US Treasury zero curve in the period 1992:01–2007:12. The autocorrelation is statistically significant for the maturities of three, five and ten years. However, the magnitude of all autocorrelations is very small, which makes them economically insignificant.

Table II: Autocorrelation of high-frequency yield changes

	2Y	3Y	5Y	7Y	10Y
Autocorrelation	0.0039	0.0154	-0.0064	-0.0040	-0.0175
p-value	(0.0648)	(0.0001)	(0.0025)	(0.0589)	(0.0001)

In a second step, we use the volatility signature plots displaying the average realized volatility against the sampling frequency (Figure 1). In the presence of microstructure noise, the average realized volatility increases with the sampling frequency. The reason is the dominance of noise at the very high-frequency sampling (see e.g., Bandi and Russell, 2008). None of the above diagnostics suggests that the microstructure noise present in our data is large and could overwhelm our results.

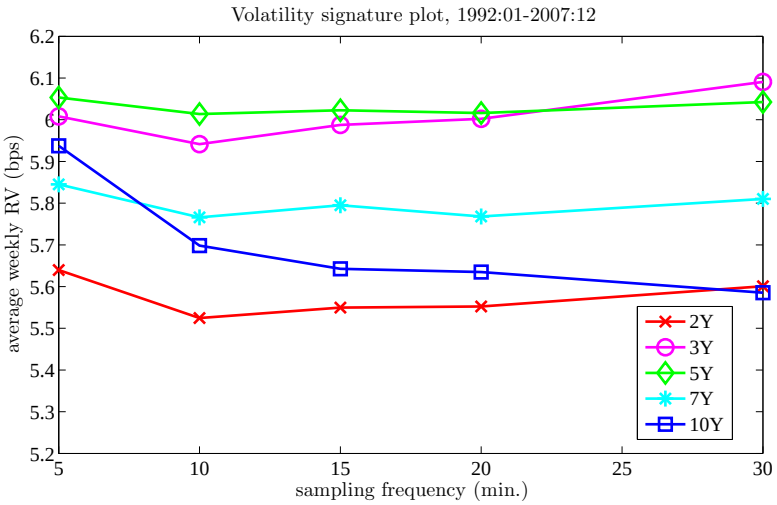

Figure 1: Volatility signature plot

We plot the average weekly realized volatility (RV) against the sampling frequency for the whole sample 1992:01–2007:12. We consider five maturities in the zero coupon curve: two, three, five, seven, and ten years.

Table III: Correlation of zero coupon yields with CMT and GSW yields

	2Y	3Y	5Y	7Y	10Y
Corr CMT	1.000	1.000	0.999	0.996	0.997
Corr GSW	1.000	0.999	0.999	0.998	0.997

I.C. Extracting zero coupon yield curve from high-frequency data

We fit the discount curve using smoothing splines. One of the important steps in the procedure is to select the appropriate number of knot points. We make the number of knot points dependent on the number of available bonds and locate them at the bond maturities. In our setting, the number of knot points varies between three and six. The fact that we consider only one specific part of the zero coupon yield curve allows us to use constant roughness penalty as in Fisher, Nychka, and Zervos (1994) for estimating the whole curve. Waggoner (1997) proposes a varying roughness penalty for the smoothing splines procedure with a low penalty at the short end and a high penalty at the very long end of the curve. In the period 2001:01–2010:12, the intraday quotes on Treasury bills are not available from the BrokerTec database. In order to anchor the very short end for the smoothing splines procedure, we include the daily data on the three-month Treasury bill obtained from the FRED database at the FRB St. Louis. Before using the constructed zero curve for the realized volatility estimation, we compare our zero coupon yields with the daily Constant Maturity Treasury rates (CMT) from the Fed, as well as with zero yields compiled by Gürkaynak, Sack, and Wright (2006) (GSW). Our daily yields are almost perfectly correlated with the CMTs as well as with the GSW yields. Table III summarizes the results.

I.D. Realized covariance matrix estimation

This section discusses the robustness and efficiency of the realized second moment estimator proposed in the paper that are critical for our results. In the paper, we use the outer product estimator given by:

$$RCov(t,t+1;N) = \sum_{i=1,\ldots,N} \left(y_{t+\frac{i}{N}} - y_{t+\frac{i-1}{N}}\right)\left(y_{t+\frac{i}{N}} - y_{t+\frac{i-1}{N}}\right)'. \quad (1)$$

In case of asynchronous trading, the realized covariance matrix estimator defined in Eq. (1) can be biased toward zero (see e.g. Hayashi and Yoshida, 2005; Audrino and Corsi, 2010). The bias is to a large extent generated by the interpolation of non-synchronously traded assets, and its severity depends on the difference in liquidity of the assets considered.[1] Hayashi and Yoshida (2005, HY) propose a covariance estimator which corrects for the bias in (1). The estimator sums up all cross-products of returns which have an overlap in their time spans, and thus no data is thrown away. The covariance of two bond yields reads:

$$RCov_{i,j}^{HY}(t, t+h; N_i, N_j) = \sum_{k=1}^{N_i} \sum_{l=1}^{N_j} \left(y_{t_i + \frac{kh}{N_i}} - y_{t_i + \frac{(k-1)h}{N_i}} \right) \left(y_{t_j + \frac{lh}{N_j}} - y_{t_j + \frac{(l-1)h}{N_j}} \right) \mathbb{I}\left(\tau_i \cap \tau_j \neq 0\right) \tag{2}$$

where τ_i and τ_j denote the interval of the return on the first and second bond, respectively.

To verify the robustness of our realized covariance estimator (1), we implement the HY approach for the realized covariance of ten- and five-year bond. Both estimators deliver very similar results in terms of magnitude and covariance dynamics. They are highly correlated (90%) and the t-test for the difference in means does not reject the null that $\mu_{\text{outer}} = \mu_{HY}$ (p-val $= 0.57$).

There at least two reasons why we stick to the simple outer-product realized covariance estimator (1). For one, estimators of Hayashi and Yoshida (2005), Audrino and Corsi (2010) are not directly applicable in our case because for the construction of the zero curve we require a synchronized set of yield changes. More importantly, on-the-run Treasury bonds are largely homogenous in terms of liquidity, which is well proxied by the average number of quotes/trades per day reported in Table I of Appendix I.B.

I.E. Constructing yield implied volatilities

We use at-the-money options on Treasury futures to obtain Black implied price volatility $IV_{n,t,T}^{Black}$. The yield implied volatility is obtained as follows (e.g. Hull, 2005):

$$IV_{n,t,T} = IV_{n,t,T}^{Black} / D_{n,t}^{c} \sqrt{\frac{NC}{NT}}, \tag{3}$$

where n is the maturity of underlying Treasury coupon bond in years, $D_{n,t}^{c}$ denotes the duration of the coupon bond with maturity n, $(T-t)$ is the maturity of the option, NC denotes the number of calendar days between t and T while NT indicates the number of trading days in the same period. Following Carr and Wu (2006), we annualize the implied volatility using the formula below:

$$NT = NC - 2 \times \text{int}(NC/7). \tag{4}$$

To obtain the weekly series used in the model estimation, we use the last business day of the week. One could consider an alternative way of constructing implied volatilities for bonds relying on the model-free methodology (Britten-Jones and Neuberger, 2000), similar to the one applied by the CBOE for the new equities VIX. This approach exploits prices of all available options across strikes, and not just at-the-money volatilities. While model-free implied volatility may have a better theoretical justification in terms of measuring the risk neutral expected variance, its construction becomes problematic in less liquid markets where the coverage of available strikes is irregular and sparse. The truncation of the strikes range in implied volatility estimates introduces a measurement error that may outweigh the theoretical advantage of the model-free approach (Andersen and Bondarenko, 2007). Since we want to cover a range of bond maturities, the at-the-money Black's volatility is likely to offer a more robust estimate of the implied volatilities in the bond market.

[1] Audrino and Corsi (2012) offer a thorough discussion of the bias in realized covariance.

I.F. Survey data

BlueChip Financial Forecasts. BlueChip Financial Forecasts (BCFF) survey contains monthly forecast of yields, inflation and GDP growth given by approximately 45 leading financial institutions. The BCFF is published on the first day of each month, but the survey itself is conducted over a two-day period, usually between the 23rd and 27th of each month. The exception is the survey for the January issue which generally takes place between the 17th and 20th of December. The precise dates as to when the survey was conducted are not published. The BCFF provides forecasts of constant maturity yields across several maturities: three and six months, one, two, five, ten, and 30 years. The short end of the term structure is additionally covered with the forecasts of the Fed funds rate, prime bank rate and three-month LIBOR rate. The forecasts are quarterly averages of interest rates for the current quarter, the next quarter out to five quarters ahead. The figures are expressed as percent per annum. In addition, panelist provide forecasts for macroeconomic quantities: real GDP, GDP price index and Consumer Price Index (CPI). The numbers are seasonally adjusted quarter-on-quarter changes.

II. Model solution

We provide solutions for the general version of the model, which incorporates both correlation between the dW and dZ shocks and a general form of the market prices of risk. In the paper, we analyze a version of the model in which the correlation parameter is set to zero.

II.A. Dependence between X and V factors

In the general case, X_t and V_t can be correlated, i.e.:

$$dZ_X = dW\rho + \sqrt{1-\rho'\rho}\, dB \tag{5}$$
$$= dW\rho + \widetilde{\rho} dB, \tag{6}$$

where dB is a (2×1)-vector of Brownian motions which is independent from dW, and ρ is a (2×1)-vector such that $\rho \in [-1,1]$ and $\rho'\rho < 1$ (e.g., da Fonseca, Grasselli, and Tebaldi, 2006; Buraschi, Porchia, and Trojani, 2010). We use short notation $\widetilde{\rho} := \sqrt{1-\rho'\rho}$.

II.B. General form of the market prices of risk

Let us write the shocks to Y under the physical dynamics as (for brevity we omit the superscript $\mathbb{P}$):

$$dZ = \begin{pmatrix} dZ_X \\ dZ_f \end{pmatrix} = \begin{pmatrix} dW\rho + \widetilde{\rho} dB \\ dZ_f \end{pmatrix} = \begin{pmatrix} dW\rho \\ 0_{1\times 2} \end{pmatrix} + \underbrace{\begin{pmatrix} \widetilde{\rho} I_{2\times 2} & 0_{2\times 1} \\ 0_{1\times 2} & 1_{1\times 1} \end{pmatrix}}_{R} \underbrace{\begin{pmatrix} dB \\ dZ_f \end{pmatrix}}_{d\widetilde{Z}} = \begin{pmatrix} dW\rho \\ 0_{1\times 2} \end{pmatrix} + R d\widetilde{Z}, \tag{7}$$

where

$$R = \begin{pmatrix} \widetilde{\rho} I_{2\times 2} & 0_{2\times 1} \\ 0_{1\times 2} & 1_{1\times 1} \end{pmatrix}, \qquad d\widetilde{Z} = \begin{pmatrix} dB \\ dZ_f \end{pmatrix}. \tag{8}$$

The change of drift is specified as:

$$d\widetilde{Z} = d\widetilde{Z}^{\mathbb{Q}} - \Lambda_{Y,t}dt \tag{9}$$

$$dW = dW^{\mathbb{Q}} - \Lambda_{V,t}dt \tag{10}$$

$$\Lambda_{Y,t} = \Sigma_Y^{-1}(V_t)\left(\lambda_Y^0 + \lambda_Y^1 Y_t\right) \tag{11}$$

$$\Lambda_{V,t} = \left(\sqrt{V_t}\right)^{-1}\Lambda_V^0 + \sqrt{V_t}\Lambda_V^1, \tag{12}$$

where λ_Y^0 and λ_Y^1 are a $(n+1)$-vector and $(n+1)\times(n+1)$ matrix of parameters, and Λ_V^0 and Λ_V^1 are $n\times n$ constant matrices. To exclude arbitrage, the market price of risk requires that the parameter matrix Q be invertible, so that V_t stays in the positive-definite domain. This specification implies the risk-neutral dynamics of Y_t given by:

$$dY_t = \left[\left(\mu_Y - \begin{pmatrix}\Lambda_V^0\rho\\ 0\end{pmatrix} - R\lambda_Y^0\right) + \left(\mathcal{K}_Y - R\lambda_Y^1\right)Y_t - \begin{pmatrix} V_t\Lambda_V^1\rho\\ 0\end{pmatrix}\right]dt + \Sigma_Y\left(V_t\right)dZ_t^{\mathbb{Q}}. \tag{13}$$

Let:

$$\mu_Y^{\mathbb{Q}} = \mu_Y - \begin{pmatrix}\Lambda_V^0\rho\\ 0\end{pmatrix} - R\lambda_Y^0 \tag{14}$$

$$\mathcal{K}_Y^{\mathbb{Q}} = \mathcal{K}_Y - R\lambda_Y^1. \tag{15}$$

The dynamics of V_t is given as:

$$dV_t = \left[\left(\Omega\Omega' - \Lambda_V^0 Q - Q'\Lambda_V^{0\prime}\right) + \left(M - Q'\Lambda_V^{1\prime}\right)V_t + V_t\left(M' - \Lambda_V^1 Q\right)\right]dt + \sqrt{V_t}dW_t^{\mathbb{Q}}Q + Q'dW_t^{\mathbb{Q}\prime}\sqrt{V_t}. \tag{16}$$

Let

$$\Omega^{\mathbb{Q}}\Omega^{\mathbb{Q}\prime} = \Omega\Omega' - \Lambda_V^0 Q - Q'\Lambda_V^{0\prime} = (k-2v)Q'Q \tag{17}$$

$$M^{\mathbb{Q}} = M - Q'\Lambda_V^{1\prime}, \tag{18}$$

where, to preserve the same distribution under $\mathbb{P}$ and $\mathbb{Q}$, we assume $\Lambda_V^0 = vQ'$ for a scalar v such that $(k-2v) > n-1$.

II.C. Solution for bond prices

Since both components of the state vector, i.e. Y_t, V_t, are affine, bond prices are of the form:

$$F\left(Y_t, V_t; t, \tau\right) = \exp\left\{A\left(\tau\right) + B\left(\tau\right)'Y_t + Tr\left[C\left(\tau\right)V_t\right]\right\}. \tag{19}$$

By discounted Feynman-Kac theorem, the drift of dF equals rF, thus:

$$\mathcal{L}_{\{Y,V\}}F + \frac{\partial F}{\partial t} = rF, \tag{20}$$

where $\mathcal{L}_{\{Y,V\}}$ is the joint infinitesimal generator of the couple $\{Y_t, V_t\}$ under the risk neutral measure. We have:

$$\mathcal{L}_{\{Y,V\}}F = \left(\mathcal{L}_Y + \mathcal{L}_V + \mathcal{L}_{Y,V}\right)F \tag{21}$$

$$\mathcal{L}_Y F = \frac{\partial F}{\partial Y'}\left[\mu_Y^{\mathbb{Q}} + \mathcal{K}_Y^{\mathbb{Q}}Y - \begin{pmatrix} V_t\Lambda_V^1\rho\\ 0\end{pmatrix}\right] + \frac{1}{2}Tr\left[\frac{\partial F}{\partial Y\partial Y'}\Sigma_Y\left(V\right)\Sigma_Y'\left(V\right)\right] \tag{22}$$

$$\mathcal{L}_V F = Tr\left[\left(\Omega^{\mathbb{Q}}\Omega^{\mathbb{Q}\prime} + M^{\mathbb{Q}}V + VM^{\mathbb{Q}\prime}\right)\mathcal{R}F + 2V\mathcal{R}Q'Q\mathcal{R}F\right] \tag{23}$$

$$\mathcal{L}_{Y,V}F = 2Tr\left[\left(\mathcal{R}Q'\rho\frac{\partial}{\partial X'}\right)FV\right]. \tag{24}$$

$\mathcal{R}$ is a matrix differential operator: $\mathcal{R}_{ij} := \left(\frac{\partial}{\partial V_{ij}}\right)$. Substituting derivatives of (19) into (20) gives:

$$B'_\tau\left(\mu_Y^{\mathbb{Q}} + \mathcal{K}_Y^{\mathbb{Q}} Y\right) - Tr\left(\Lambda_V^1 \rho B'_{X,\tau} V\right) + \frac{1}{2} Tr\left(B_{X,\tau} B'_{X,\tau} V\right) + \frac{1}{2} B_{f,\tau}^2 \sigma_f^2 \tag{25}$$

$$+ Tr\left(\Omega^{\mathbb{Q}} \Omega^{\mathbb{Q}\prime} C_\tau\right) + Tr\left[\left(C_\tau M^{\mathbb{Q}} + M^{\mathbb{Q}\prime} C_\tau + 2 C_\tau Q' Q C_\tau\right) V\right] \tag{26}$$

$$+ Tr\left[\left(C_\tau Q' \rho B'_{X,\tau} + B_{X,\tau} \rho' Q C_\tau\right) V\right] \tag{27}$$

$$= \frac{\partial A_\tau}{\partial \tau} + \frac{\partial B_\tau}{\partial \tau}' Y + Tr\left(\frac{\partial C_\tau}{\partial \tau} V\right) + \gamma_0 + \gamma_Y' Y \tag{28}$$

By matching coefficients, we obtain the system of equations:

$$\frac{\partial A}{\partial \tau} = B'_\tau \mu_Y^{\mathbb{Q}} + \frac{1}{2} B_{f,\tau}^2 \sigma_f^2 + Tr\left(\Omega^{\mathbb{Q}} \Omega^{\mathbb{Q}\prime} C_\tau\right) - \gamma_0 \tag{29}$$

$$\frac{\partial B}{\partial \tau} = \mathcal{K}^{\mathbb{Q}\prime} B_\tau - \gamma_Y \tag{30}$$

$$\frac{\partial C}{\partial \tau} = \frac{1}{2} B_{X,\tau} B'_{X,\tau} + C_\tau\left(M^{\mathbb{Q}} + Q' \rho B'_{X,\tau}\right) + \left(M^{\mathbb{Q}\prime} + B_{X,\tau} \rho' Q\right) C_\tau + 2 C_\tau Q' Q C_\tau - \Lambda_V^1 \rho B'_{X,\tau} \tag{31}$$

To obtain the solution provided in the text, set $\rho = 0_{2\times 1}$.

II.D. Instantaneous volatility of yields

The instantaneous volatility of yields is given as:

$$\frac{1}{dt}\left\langle dy_t^{\tau_1}, dy_t^{\tau_2}\right\rangle = \frac{1}{\tau_1 \tau_2} Tr\left[B_{f,\tau_2} B_{f,\tau_1} \sigma_f^2 + \left(B_{X,\tau_1} B'_{X,\tau_2} + 2 C_{\tau_2} Q' \rho B'_{X,\tau_1} + 2 C_{\tau_1} Q' \rho B'_{X,\tau_2} + 4 C_{\tau_1} Q' Q C_{\tau_2}\right) V_t\right]. \tag{32}$$

Proof. The only term which requires clarification is $B'_{\tau_1} dY_t \times Tr\left[C_{\tau_2} dV_t\right] = B'_{X,\tau_1} dX_t \times Tr\left[C_{\tau_2} dV_t\right]$

$$\begin{aligned} B'_{X,\tau_1} dX_t \times Tr\left[C_{\tau_2} dV_t\right] &= B'_{X,\tau_1} \sqrt{V} dZ_X \times Tr\left[C_{\tau_2}\left(\sqrt{V} dW Q + Q' dW' \sqrt{V}\right)\right] \\ &= B'_{X,\tau_1} \sqrt{V}\left(dW \rho + \widetilde{\rho} dB\right) \times 2 Tr\left(Q C_{\tau_2} \sqrt{V} dW\right) \\ &= 2 Tr\left(C_{\tau_2} Q' \rho B'_{X,\tau_1} V\right) \end{aligned}$$

Where we use the following fact:

$$Tr\left[C\left(\sqrt{V} dW Q + Q' dW' \sqrt{V}\right)\right] = 2 Tr\left(Q C \sqrt{V} dW\right). \tag{33}$$

□

II.E. Conditional covariance of X and V

We consider the conditional covariance matrix of X and V

$$d\left\langle \begin{pmatrix} X_{t,1} \\ X_{t,2} \\ f_t \end{pmatrix}, \begin{pmatrix} V_{t,11} \\ V_{t,12} \\ V_{t,22} \end{pmatrix} \right\rangle = \begin{pmatrix} d\left(X_1, V_{11}\right) & d\left(X_1, V_{12}\right) & d\left(X_1, V_{22}\right) \\ d\left(X_2, V_{11}\right) & d\left(X_2, V_{12}\right) & d\left(X_2, V_{22}\right) \\ d\left(f, V_{11}\right) & d\left(f, V_{12}\right) & d\left(f, V_{22}\right) \end{pmatrix} \tag{34}$$

The elements of the covariance matrix are given by:

$$d\langle X_k, V_{ij}\rangle = \rho' \left(Q_{:,j} V_{ik} + Q_{:,i} V_{jk}\right), \tag{35}$$

where $Q_{:,j}$ denotes the j-th column of matrix Q.

Proof. The expression follows by simple algebra:

$$\begin{aligned}
\frac{1}{dt} d\langle V_{ij}, X_k\rangle &= \left[e_i' \left(\sqrt{V} dW Q\right) e_j + e_i' \left(Q' dW' \sqrt{V}\right) e_j\right] \left(e_k' \sqrt{V} dW \rho\right) \\
&= Tr\left(e_j e_i' \sqrt{V} dW Q\right) \times Tr\left(\rho e_k' \sqrt{V} dW\right) + Tr\left(e_j e_i' Q' dW' \sqrt{V}\right) \times Tr\left(\rho e_k' \sqrt{V} dW\right) \\
&= \mathrm{vec}\left(\sqrt{V} e_i e_j' Q'\right)' \mathrm{vec}\left(\sqrt{V} e_k \rho'\right) + \mathrm{vec}\left(\sqrt{V} e_j e_i' Q'\right)' \mathrm{vec}\left(\sqrt{V} e_k \rho'\right) \\
&= Tr\left(Q e_j e_i' V e_k \rho'\right) + Tr\left(Q e_i e_j' V e_k \rho'\right) \\
&= \rho' \left(Q_{:,j} V_{ik} + Q_{:,i} V_{jk}\right),
\end{aligned} \tag{36}$$

where e_i is the i-th column of the identity matrix. □

II.F. Moments of the state variables

This section derives moments of the state variables necessary for the implementation of the unscented Kalman filter.

II.F.1. Moments of the V_t process

The first conditional moment of the volatility process V_t is given as:

$$E_t\left(V_{t+\Delta t}\right) = k\bar{\mu}_{V,\Delta t} + \Phi_{V,\Delta t} V_t \Phi_{V,\Delta t}', \tag{37}$$

where

$$\Phi_{V,\Delta t} = e^{M\Delta t} \tag{38}$$

$$\bar{\mu}_{V,\Delta t} = \int_0^{\Delta t} e^{Ms} Q'Q e^{M's} ds = -\frac{1}{2} \hat{C}_{12}(\Delta t) \hat{C}_{11}'(\Delta t), \tag{39}$$

with

$$\begin{pmatrix} \hat{C}_{11}(\Delta t) & \hat{C}_{12}(\Delta t) \\ \hat{C}_{21}(\Delta t) & \hat{C}_{22}(\Delta t) \end{pmatrix} = \exp\left[\Delta t \begin{pmatrix} M & -2Q'Q \\ 0 & -M' \end{pmatrix}\right].$$

See Van Loan (1978) for the derivation of the above expression. Assuming stationarity (i.e. negative eigenvalues of M), the unconditional first moment of V_t follows as:

$$\lim_{\Delta t \to \infty} \mathrm{vec} E_t\left(V_{t+\Delta t}\right) = k\mathrm{vec}\left(\bar{\mu}_{V,\infty}\right) = -k\left[(I \otimes M) + (M \otimes I)\right]^{-1} \mathrm{vec}(Q'Q). \tag{40}$$

The conditional and unconditional covariance matrix of V_t reads:

$$Cov_t\left[\mathrm{vec}\left(V_{t+\Delta t}\right)\right] = \left(I_{n^2} + K_{n,n}\right)\left[\Phi_{V,\Delta t} V_t \Phi_{V,\Delta t}' \otimes \bar{\mu}_{V,\Delta t} + k\left(\bar{\mu}_{V,\Delta t} \otimes \bar{\mu}_{V,\Delta t}\right) + \bar{\mu}_{V,\Delta t} \otimes \Phi_{V,\Delta t} V_t \Phi_{V,\Delta t}'\right]. \tag{41}$$

$$\lim_{\Delta t \to \infty} Cov_t\left[\mathrm{vec}\left(V_{t+\Delta t}\right)\right] = \left(I_{n^2} + K_{n,n}\right) k\left(\bar{\mu}_{V,\infty} \otimes \bar{\mu}_{V,\infty}\right). \tag{42}$$

$K_{n,n}$ is the commutation matrix with the property that $K_{n,n}\mathrm{vec}(A) = \mathrm{vec}(A')$. These moments are derived in Buraschi, Cieslak, and Trojani (2010) and thus are stated without a proof.

Gourieroux, Jasiak, and Sufana (2009) show that when $\Omega\Omega' = kQ'Q$, k integer, the dynamics of V_t can be represented as the sum of outer products of k independent Ornstein-Uhlenbeck processes with a zero long-run mean:

$$V_t = \sum_{i=1}^{k} v_t^i v_t^{i\prime} \tag{43}$$

$$v_{t+\Delta t}^i = \Phi_{V,\Delta t} v_t^i + \epsilon_{t+\Delta t}^i, \quad \epsilon_t^i \sim N(0, \bar{\mu}_{V,\Delta t}). \tag{44}$$

Taking the outer-product implies that the exact discretization of V_t has the form:

$$V_{t+\Delta t} = k\bar{\mu}_{V,\Delta t} + \Phi_{V,\Delta t} V_t \Phi'_{V,\Delta t} + u_{t+\Delta t}^V, \tag{45}$$

where the shock $u_{t+\Delta t}^V$ is a heteroskedastic martingale difference sequence.

II.F.2. Moments of the Y_t dynamics

We assume that the dimension of X_t is $n = 2$ and f_t is a scalar process. Let $Y_t = (X_t', f_t)'$:

$$dY_t = (\mu_Y + \mathcal{K}_Y Y_t)\, dt + \Sigma(V_t)\, dZ_t. \tag{46}$$

It is straightforward to show that the conditional and unconditional first moment of Y_t has the form:

$$E_t(Y_{t+\Delta t}) = \left(e^{\mathcal{K}_Y \Delta t} - I\right) \mathcal{K}_Y^{-1} \mu_Y + e^{\mathcal{K}_Y \Delta t} Y_t \tag{47}$$

$$\lim_{\Delta t \to \infty} E_t(Y_{t+\Delta t}) = -\mathcal{K}_Y^{-1} \mu_Y, \tag{48}$$

where $\mathcal{K}_Y$ is assumed to be lower triangular with negative eigenvalues.

To compute the conditional covariance of Y_t, let $V_Y(t,T) := Cov_t(Y_T)$. Following Fisher and Gilles (1996), the application of Ito's lemma to $\hat{Y}(t,T) := E_t(Y_T)$ reveals that:

$$d\hat{Y}(t,T) = \hat{\sigma}_Y(t,T)\, dZ_t, \tag{49}$$

where $\hat{\sigma}_Y(t,T) := \Phi_Y(t,T)\Sigma(V_t)$, with

$$\Phi_Y(t,T) = e^{\mathcal{K}_Y(T-t)} \tag{50}$$

and

$$\Sigma_Y(V_t) = \begin{pmatrix} \sqrt{V_t} & 0 \\ 0 & \sigma_f \end{pmatrix}. \tag{51}$$

Then, integrating $d\hat{Y}(t,T)$ yields:

$$Y_T = \hat{Y}_{T,T} = \hat{Y}_{t,T} + \int_{s=t}^{T} \hat{\sigma}_Y(s,T)\, dZ_s. \tag{52}$$

Therefore, we have:

$$V_Y(t,T) = Cov_t\left[\int_{s=t}^{T} \hat{\sigma}_Y(s,T) dZ_s^Y\right] = E_t\left[\int_{s=t}^{T} \hat{\sigma}_Y(s,T)\hat{\sigma}_Y(s,T)' ds\right] \tag{53}$$

$$= \int_{s=t}^{T} \Phi_Y(s,T) E_t \begin{pmatrix} V_s & 0 \\ 0 & \sigma_f^2 \end{pmatrix} \Phi'_Y(s,T) ds. \tag{54}$$

Note that since $\mathcal{K}_Y$ is lower triangular, $\Phi_Y(t,T) = e^{\mathcal{K}_Y(T-t)}$ is also lower triangular, and we have:

$$\Phi_Y(t,T) = \begin{pmatrix} \Phi_X(t,T) & 0 \\ \Phi_{Xf}(t,T) & \Phi_f(t,T) \end{pmatrix}. \tag{55}$$

Let us for convenience define two matrices:

$$\mathcal{M}_{1Y}(t,T) = \begin{pmatrix} \Phi_X(t,T)\otimes\Phi_X(t,T) \\ \Phi_X(t,T)\otimes\Phi_{fX}(t,T) \\ \Phi_{fX}(t,T)\otimes\Phi_X(t,T) \\ \Phi_{fX}(t,T)\otimes\Phi_{fX}(t,T) \end{pmatrix} \text{ and } \mathcal{M}_{0Y} = \begin{pmatrix} 0_{8\times 1} \\ \Phi_f^2(t,T)\sigma_f^2 \end{pmatrix}. \tag{56}$$

With help of simple matrix algebra applied to (54), the conditional covariance of Y_t has the (vectorized) form

$$\text{vec}V_Y(t,T) = \int_{s=t}^{T} \mathcal{M}_{1Y}(s,T)\left[\Phi_V(s,T)\otimes\Phi_V(s,T)\right]ds \times \text{vec}\left(V_t\right) \tag{57}$$

$$+ \int_{s=t}^{T} k\mathcal{M}_{1Y}\text{vec}\left[\bar{\mu}_V(t,s)\right]ds + \int_{s=t}^{T}\mathcal{M}_{0Y}(s,T)ds. \tag{58}$$

The unconditional covariance of Y is given as:

$$\lim_{T\to\infty}\text{vec}V_Y(t,T) = \lim_{T\to\infty}\int_{s=t}^{T} k\mathcal{M}_{1Y}(s,T)\text{vec}\left[\bar{\mu}_V(t,s)\right]ds + \int_{s=t}^{T}\mathcal{M}_{0Y}(s,T)ds. \tag{59}$$

This expression exists if the mean reversion matrices M and $\mathcal{K}_Y$ are negative definite.

The expressions for the conditional mean (47) and covariance (58) give rise to an exact discretization of the process Y_t.

Remark 1. In order to avoid the numerical integration, we can resort to a discrete-time approximation of the unconditional covariance matrix of Y factors. To this end, we discretize the dynamics

$$dY_t = \left(\mu_Y + \mathcal{K}_Y Y_t\right)dt + \Sigma_Y\left(V_t\right)dZ_t \tag{60}$$

as

$$Y_{t+\Delta t} = \bar{\mu}_{Y,\Delta t} + \Phi_{Y,\Delta t}Y_t + \Sigma_Y\left(V_t\right)\sqrt{\Delta t}\varepsilon_{t+\Delta t}, \tag{61}$$

where $\bar{\mu}_{Y,\Delta t} = \left(e^{\mathcal{K}_Y\Delta t} - I\right)\mathcal{K}_Y^{-1}\mu_Y$. The second moment of the discretized dynamics is straightforward to obtain as:

$$\begin{aligned} \text{vec}E\left(YY'\right) &= \left(I - \Phi_{Y,\Delta t}\otimes\Phi_{Y,\Delta t}\right)^{-1}\times \\ &\times\text{vec}\left\{\bar{\mu}_{Y,\Delta t}\bar{\mu}'_{Y,\Delta t} + \bar{\mu}_{Y,\Delta t}E\left(Y'\right)\Phi'_{Y,\Delta t} + \Phi_{Y,\Delta t}E\left(Y\right)\bar{\mu}'_{Y,\Delta t} + E\left[\Sigma_Y\left(V_t\right)\Sigma_Y\left(V_t\right)'\right]\Delta t\right\} \\ \text{vec}\left[Var\left(Y\right)\right] &= \text{vec}E\left(YY'\right) - \text{vec}E\left(Y\right)\left[\text{vec}E\left(Y\right)\right]'. \end{aligned} \tag{62}$$

We check that for the weekly discretization step $\Delta t = \frac{1}{52}$ this approximation works well, and implies a significant reduction of the computational time.

II.G. Discrete approximation to the unconditional covariance matrix of X and V

We can use the discretized dynamics of X and V to compute the unconditional covariance matrix:

$$X_{t+\Delta t} = \bar{\mu}_{X,\Delta t} + \Phi_{X,\Delta t}X_t + \sqrt{V_t\Delta t}\left(U_{t+\Delta t}\rho + \widetilde{\rho}b_{t+\Delta t}\right) \tag{63}$$

$$V_{t+\Delta t} = k\bar{\mu}_{V,\Delta t} + \Phi_{V,\Delta t}V_t\Phi'_{V,\Delta t} + \sqrt{V_t\Delta t}U_{t+\Delta t}Q + Q'U'_{t+\Delta t}\sqrt{V_t\Delta t}, \tag{64}$$

where U_t is a 2×2 matrix of Gaussian shocks, and b_t is a 2-vector of Gaussian shocks. The covariance between X and V is computed as :

$$Cov\left[X, \text{vec}(V)\right] = E\left[X\text{vec}\left(V\right)'\right] - E\left(X\right)E\left[\text{vec}\left(V\right)'\right]. \tag{65}$$

The element $E\left[X\text{vec}\left(V\right)'\right]$ reads:

$$\text{vec}E\left[X\left(\text{vec}V\right)'\right] = \left[I_{n^3} - \left(\Phi_V \otimes \Phi_V\right) \otimes \Phi_X\right]^{-1}\left(\text{vec}A + \text{vec}B\right), \tag{66}$$

where A is given as:

$$A = \bar{\mu}_X \text{vec}\left(k\bar{\mu}_V\right)' + \bar{\mu}_X \text{vec}\left[\Phi_V E\left(V_t\right)\Phi_V'\right] + \Phi_X E(X_t)\text{vec}(k\bar{\mu}_V)', \tag{67}$$

and the elemtent (k, ij) of matrix B, associated with the covariance of X_k and V_{ij} has the form:

$$B_{k,ij} = \rho'\left(Q_{:,j}V_{ik} + Q_{:,i}V_{jk}\right)\Delta t, \tag{68}$$

where $B = \begin{pmatrix} B_{1,11} & B_{1,12} & B_{1,21} & B_{1,22} \\ B_{2,11} & B_{2,12} & B_{2,21} & B_{2,22} \end{pmatrix}$. Note that the second and third columns of B are identical.

III. Model estimation

III.A. Discretization and vectorization of the state space

This section collects the details about the vectorization of transition dynamics for Y_t and V_t.

The transition equation for Y_t is specified as an Euler approximation of the physical dynamics given by equation (5) in the paper:

$$Y_{t+\Delta t} = \bar{\mu}_{Y,\Delta t} + \Phi_{Y,\Delta t}Y_t + u^Y_{t+\Delta t}, \tag{69}$$

where u^Y_t is a vector of heteroskedastic innovations $u^Y_t = \Sigma_Y(V_t)\sqrt{\Delta t}\epsilon_{t+\Delta t}$. The transition equation for the matrix process V_t is obtained by an exact discretization of the dynamics (3) in the body of the paper:

$$V_{t+\Delta t} = k\bar{\mu}_{V,\Delta t} + \Phi_{V,\Delta t}V_t\Phi'_{V,\Delta t} + u^V_{t+\Delta t}, \tag{70}$$

where u^V_t represents a symmetric matrix of heteroskedastic innovation. $\bar{\mu}_{Y,\Delta t}$, $\mu_{V,\Delta t}$, $\Phi_{Y,\Delta t}$ and $\Phi_{V,\Delta t}$ are explicit functions of the continuous-time parameters.

Parameters for discretized transition dynamics of Y_t are given by:

$$\bar{\mu}_{Y,\Delta t} = \left(e^{\mathcal{K}_Y\Delta t} - I\right)\mathcal{K}_Y^{-1}\mu_Y \tag{71}$$

$$\Phi_{Y,\Delta t} = e^{\mathcal{K}_Y\Delta t}. \tag{72}$$

Parameter matrices $\Phi_{V,\Delta t}$ and $\bar{\mu}_{V,\Delta t}$ for discretized transition dynamics of V_t are given by:

$$\bar{\mu}_{V,\Delta t} = \int_0^{\Delta t} \Phi_{V,s}Q'Q\Phi'_{V,s}ds \tag{73}$$

$$\Phi_{V,\Delta t} = e^{M\Delta t}, \tag{74}$$

The closed form solution for the integral $\bar{\mu}_{V,\Delta t}$ is given by $\int_0^{\Delta t}\Phi_{V,s}Q'Q\Phi'_{V,s}ds = -\hat{C}_{12}(\Delta t)\hat{C}'_{11}(\Delta t)$, where

$$\begin{pmatrix} \hat{C}_{11}(\Delta t) & \hat{C}_{12}(\Delta t) \\ \hat{C}_{21}(\Delta t) & \hat{C}_{22}(\Delta t) \end{pmatrix} = \exp\left[\Delta t\begin{pmatrix} M & -Q'Q \\ 0 & -M' \end{pmatrix}\right].$$

See Van Loan (1978) for the proof.

We recast the discretized covariance matrix dynamics V_t in a vector form:

$$\text{vec}(V_{t+\Delta t}) = k\text{vec}(\bar{\mu}_{V,\Delta t}) + (\Phi_{V,\Delta t} \otimes \Phi_{V,\Delta t})\text{vec}(V_t) + \text{vec}(u^V_{t+\Delta t}). \tag{75}$$

Since the process V_t lives in the space of symmetric matrices, its lower triangular part preserves all information. Let us for convenience define two linear transformations of some symmetric matrix A: (i) an elimination matrix: $\mathcal{E}_n\text{vec}(A) = \text{vech}(A)$, where $\text{vech}(\cdot)$ denotes half-vectorization, (ii) a duplication matrix: $\mathcal{D}_n\text{vech}(A) = \text{vec}(A)$. Using half-vectorization, we define $\bar{V}_t := \text{vech}(V_t) = \mathcal{E}_n\text{vec}(V_t)$, which contains $\bar{n} = n(n+1)/2$ unique elements of V_t:

$$\bar{V}_{t+\Delta t} = k\mathcal{E}_n\text{vec}(\bar{\mu}_{V,\Delta t}) + \mathcal{E}_n(\Phi_{V,\Delta t} \otimes \Phi_{V,\Delta t})\mathcal{D}_n\bar{V}_t + \mathcal{E}_n\text{vec}(u^V_{t+\Delta t}). \tag{76}$$

Collecting all elements, we can redefine the state as: $S_t = (Y_t', \bar{V}_t')'$, whose transition is described by the conditional mean:

$$E_t\left(S_{t+\Delta t}\right) = \begin{pmatrix} \left(e^{\mathcal{K}_Y \Delta t} - I\right)\mathcal{K}_Y^{-1}\mu_Y + e^{\mathcal{K}_Y \Delta t}Y_t \\ k\mathcal{E}_n\text{vec}(\bar{\mu}_{V,\Delta t}) + \mathcal{E}_n(\Phi_{V,\Delta t} \otimes \Phi_{V,\Delta t})\mathcal{D}_n\bar{V}_t \end{pmatrix}, \tag{77}$$

and the conditional covariance of the form:

$$Cov_t\left(S_{t+\Delta t}\right) = \begin{pmatrix} Cov_t(Y_{t+\Delta t}) & 0_{n\times\bar{n}} \\ 0_{\bar{n}\times n} & Cov_t\left(\bar{V}_{t+\Delta t}\right) \end{pmatrix}. \tag{78}$$

The block diagonal structure in the last expression follows from our assumption that shocks in Y_t be independent of shocks in V_t. The respective blocks are given as:

$$Cov_t(Y_{t+\Delta t}) = \Sigma_Y(V_t)\Sigma_Y(V_t)'\Delta t \tag{79}$$

$$\begin{aligned} Cov_t\left(\bar{V}_{t+\Delta t}\right) &= \mathcal{E}_n Cov_t\left(V_{t+\Delta t}\right)\mathcal{E}_n' \\ &= \mathcal{E}_n\left(I_{n^2} + K_{n,n}\right)\left[\Phi_{V,\Delta t}V_t\Phi_{V,\Delta t}' \otimes \bar{\mu}_{V,\Delta t} + k\left(\bar{\mu}_{V,\Delta t} \otimes \bar{\mu}_{V,\Delta t}\right) + \bar{\mu}_{V,\Delta t} \otimes \Phi_{V,\Delta t}V_t\Phi_{V,\Delta t}'\right]\mathcal{E}_n', \end{aligned} \tag{80}$$

where $K_{n,n}$ denotes a commutation matrix (see e.g., Magnus and Neudecker, 1979). Buraschi, Cieslak, and Trojani (2010) provide the derivation of the last expression.

III.B. Econometric identification

This section details our econometric identification procedure and parameter restrictions. To ensure econometric identification, we consider invariant model transformations of the type $\tilde{Y}_t = v + LY_t$ and $\tilde{V}_t = LV_tL'$, for a scalar v and an invertible matrix L. Such transformations result in the equivalence of the state variables, the short rate and thus yields (Dai and Singleton, 2000). If allowed, they can invalidate the results of an estimation.

To prevent the invariance, we adopt several normalizations for the risk-neutral $\mathbb{Q}$ dynamics of the process Y_t: (i) Setting $\mu_Y^{\mathbb{Q}} = 0$ allows to treat γ_0 as a free parameter. (ii) Restricting $\gamma_f = 1$ makes σ_f identified. (iii) Since both $\mathcal{K}_X$ and V_t determine interactions between the elements of X_t, they are not separately identifiable. We set $\mathcal{K}_X^{\mathbb{Q}}$ to a diagonal matrix, and allow correlations of the X_t factors to be generated solely by V_t. By the same token, the last row of matrix $\mathcal{K}_Y^{\mathbb{Q}}$, i.e. $\left(\mathcal{K}_{fX}^{\mathbb{Q}}, \mathcal{K}_f^{\mathbb{Q}}\right)$ is left unrestricted, as f_t does not interact with X_t via the diffusion term.

The identification of volatility factors V_t is ensured with three restrictions: (i) $M^{\mathbb{Q}}$ is lower triangular and (ii) Q is diagonal with positive elements. (iii) The diagonal elements of Q are uniquely determined by setting $\gamma_X = \mathbf{1}_{n\times 1}$, where $\mathbf{1}_{n\times 1}$ is a vector of ones. These normalizations protect V_t against affine transformations and orthonormal rotations of Brownian motions. Finally, to guarantee the stationarity of the state, we require that the mean reversion matrices $\mathcal{K}_Y^{\mathbb{Q}}$ and $M^{\mathbb{Q}}$ be negative definite. Due to the lower triangular structure of both, this is equivalent to restricting the diagonal elements of each matrix to be negative.

III.C. Implementation of the filter

This section summarizes the algorithm for the unscented Kalman filtering. We recast the transition and measurement equations above into one state space. The compound transition equation is given by:

$$S_{t+\Delta t} = A + BS_t + \varepsilon_{t+\Delta t}, \tag{81}$$

and the compound measurement equation is given by:

$$m_t = h(S_t; \Theta) + \vartheta_t. \tag{82}$$

$S_t = (Y_t', \bar{V}_t')'$ and A are $(n + \bar{n} + 1) \times 1$-dimensional vectors, A is given by:

$$A = \begin{pmatrix} (\Phi_{Y,\Delta t} - I)\, \mathcal{K}_Y^{-1} \mu_Y \\ k \cdot \mathcal{E}_n vec(\bar{\mu}_{V,\Delta t}) \end{pmatrix}. \tag{83}$$

B is a block-diagonal matrix of the form:

$$B = \begin{pmatrix} \Phi_{Y,\Delta t} & \mathbf{0}_{n\times\bar{n}} \\ \mathbf{0}_{\bar{n}\times n} & \mathcal{E}_n(\Phi_{V,\Delta t} \otimes \Phi_{V,\Delta t})\mathcal{D}_n \end{pmatrix}. \tag{84}$$

The vector shocks is of the form:

$$\varepsilon_{t+\Delta t} = \begin{pmatrix} u^Y_{t+\Delta t} \\ \mathcal{E}_n \mathrm{vec}(u^V_{t+\Delta t}) \end{pmatrix}, \tag{85}$$

and its covariance matrix is given by a block-diagonal matrix:

$$Cov_t(\varepsilon_{t+\Delta t}) = \begin{pmatrix} Cov_t(Y_{t+\Delta t}) & \mathbf{0}_{n\times\bar{n}} \\ \mathbf{0}_{\bar{n}\times n} & Cov_t(\bar{V}_{t+\Delta t}) \end{pmatrix}. \tag{86}$$

m_t is a vector of observed yields and volatility measures given by $m_t = (y_t^\tau, v_t^{\tau_i,\tau_j}, v_{t,t+4}^{\mathbb{Q},\tau})'$. Model implied yields and volatilities are affine in the state vector. Function $h(\cdot)$ translates the state variables to model implied yields and volatilities:

$$h(S_t; \Theta) = \begin{pmatrix} f_1(S_t; \Theta) \\ f_2(V_t; \Theta) \\ f_3(V_t; \Theta) \end{pmatrix}. \tag{87}$$

The vector of measurement errors:

$$\vartheta_t = \begin{pmatrix} \sqrt{R_1} e_{1,t} \\ \sqrt{R_2} e_{2,t} \\ \sqrt{R_3} e_{3,t} \end{pmatrix} \tag{88}$$

is Gaussian with the covariance matrix, for six yields and three volatility measurements, is given by:

$$Cov(\vartheta_t) = \begin{pmatrix} \sigma_y^2 \mathbf{I}_6 & \mathbf{0}_{6\times 7} \\ \mathbf{0}_{7\times 6} & diag(\sigma_{i,v}^2)_{i=1,\ldots,7} \end{pmatrix}. \tag{89}$$

The core of UKF is the unscented transformation which approximates a distribution of a nonlinear transformation of any random variable by a set of sample points. In the UKF framework, we apply the unscented transformation recursively to B and $h(\cdot)$.

We define $L_S := n + \bar{n} + 1$. Assume that we know the mean $\bar{S}$ and the covariance P_S of S_t at each point in time t. We form a matrix $\mathcal{S}$ of $2L_S + 1$ sigma vectors:

$$\mathcal{S}_0 = \bar{S} \tag{90}$$

$$\mathcal{S}_i = \bar{S} + \left(\sqrt{(L_S + \lambda)P_S}\right)_i, i = 1, ..., L_S \tag{91}$$

$$\mathcal{S}_i = \bar{S} - \left(\sqrt{(L_S + \lambda)P_S}\right)_{i-L_S}, i = L_S + 1, ..., 2L_S, \tag{92}$$

where $\lambda = \alpha^2(L_S - \kappa) - L_S$ is a scaling parameter governing the spread of sigma points around the mean and $\left(\sqrt{(L_S + \lambda)P_S}\right)_i$ is the i-th column of matrix P_S. Sigma points $\mathcal{S}$ are propagated through function $h(\cdot)$ to get $\mathcal{M}$. The first two moments of m_t are approximated by:

$$\bar{m} \approx \sum_{i=0}^{2L_S} W_i^{\mu} \mathcal{M}_i \tag{93}$$

$$P_S \approx \sum_{i=0}^{2L_S} W_i^{\sigma} (\mathcal{M}_i - \bar{m})(\mathcal{M}_i - \bar{m})', \tag{94}$$

where W^{μ} and W^{σ} denote weights for the mean and the covariance matrix, respectively and are defined as:

$$W_0^{\mu} = \frac{\lambda}{L_S + \lambda} \tag{95}$$

$$W_0^{\sigma} = \frac{\lambda}{L_S + \lambda} + 1 - \alpha^2 + \beta, i = 1, ..., L_S \tag{96}$$

$$W_i^{\mu} = W_i^{\sigma} = \frac{\lambda}{2(L_S + \lambda)}, i = L_S + 1, ..., 2L_S. \tag{97}$$

Parameters α and β, mainly determine higher moments of the distribution.

The UKF Algorithm

1. Initialize at unconditional moments:[2]

$$\hat{S}_0 = \mathbb{E}[S_0] \tag{98}$$

$$P_{S0} = \mathbb{E}[(S_0 - \hat{S}_0)(S_0 - \hat{S}_0)'] \tag{99}$$

   for $k \in 1, ..., \infty$:

2. Compute the sigma points:

$$\mathcal{S}_{k-1} = \left[\begin{array}{ccc} \hat{S}_{k-1} & \hat{S}_{k-1} + \sqrt{(L_S + \lambda)P_{S,k-1}} & \hat{S}_{k-1} - \sqrt{(L_S + \lambda)P_{S,k-1}} \end{array} \right] \tag{100}$$

3. Time update:

$$\mathcal{S}^a_{k|k-1} = B(\mathcal{S}_{k-1}) \tag{101}$$

$$\hat{S}_k^- = \sum_{i=0}^{2L_S} W_i^{\mu} \mathcal{S}^a_{k|k-1} \tag{102}$$

$$P_{Sk}^- = \sum_{i=0}^{2L_S} W_i^{\sigma} (\mathcal{S}^a_{ik|k-1} - \hat{S}_k^-)(\mathcal{S}^a_{ik|k-1} - \hat{S}_k^-)' + Cov_t(\varepsilon_{t+\Delta t}) \tag{103}$$

[2]We borrow the algorithm from Wan and van der Merwe (2001).

4. Augment sigma points:

$$\mathcal{S}_{k|k-1} = \left[\begin{array}{ccc} \mathcal{S}^a_{k|k-1} & \mathcal{S}^a_{0k|k-1} + \sqrt{(L_S+\lambda)Cov_t(\varepsilon_{t+\Delta t})} & \mathcal{S}^a_{0k|k-1} - \sqrt{(L_S+\lambda)Cov_t(\varepsilon_{t+\Delta t})} \end{array} \right] \tag{104}$$

$$\mathcal{M}_{k|k-1} = h(\mathcal{S}_{k|k-1}) \tag{105}$$

$$\hat{m}^-_k = \sum_{i=1}^{2L_S} W^\sigma_i \mathcal{M}_{i,k|k-1} \tag{106}$$

5. Measurement equations update:

$$P^-_{m_k} = \sum_{i=0}^{2L_S} W^\sigma_i (\mathcal{M}_{ik|k-1} - \hat{m}^-_k)(\mathcal{M}_{ik|k-1} - \hat{m}^-_k)' + Cov_t(\vartheta_{t+\Delta t}) \tag{107}$$

$$P_{S_k m_k} = \sum_{i=0}^{2L_S} W^\sigma_i (\mathcal{S}_{ik|k-1} - \hat{S}^-_k)(\mathcal{M}_{ik|k-1} - \hat{m}^-_k)' \tag{108}$$

$$\mathcal{K}_k = P_{S_k m_k} P^{-1}_{m_k} \tag{109}$$

$$\hat{F}_k = \hat{F}^-_k + \mathcal{K}_k(m_k - \hat{m}^-_k) \tag{110}$$

$$P_k = P^-_k - \mathcal{K}_k P^-_{m_k} \mathcal{K}'_k. \tag{111}$$

III.D. Pseudo-maximum likelihood estimation

Collecting all measurements in vector m_{t+1}, let $\hat{m}^-_{t+1}$ and $\hat{P}^-_{m,t+1}$ denote the time-t forecasts of the time-$(t+1)$ values of the measurement series and of their conditional covariance, respectively, as returned by the filter (for convenience 1 means one week). By normality of measurement errors, we can compute the quasi-log likelihood value for each time point in our sample:

$$l_{t+1}(\Theta) = -\frac{1}{2}\ln|P^-_{m,t+1}| - \frac{1}{2}\left(\hat{m}^-_{t+1} - m_{t+1}\right)'\left(P^-_{m,t+1}\right)^{-1}\left(\hat{m}^-_{t+1} - m_{t+1}\right), \tag{112}$$

and obtain parameter estimates by maximizing the criterion:

$$\hat{\Theta} := \arg\min_{\Theta} \mathcal{L}\left(\Theta, \{m_t\}_{t=1}^T\right) \quad \text{with} \quad \mathcal{L}\left(\Theta, \{m_t\}_{t=1}^T\right) = \sum_{t=0}^{T-1} l_{t+1}(\Theta). \tag{113}$$

with $T = 999$ weeks. The initial log-likelihood is evaluated at the unconditional moments of the state vector (see Section II.F for the expressions).

IV. Estimation results

Table IV reports parameter estimates and the corresponding standard errors for the model outlined in Section II in the body of the paper. At the bottom of the table, we report the contributions of yields, realized and implied volatility to the likelihood function. Table V reports the in-sample fit of the model to yields, realized and implied volatilities.

Table IV: Parameter estimates

This table reports parameter estimates for the baseline model outlined in Section II in the body of the paper. Panel A reports the yield curve parameter estimates and Panel B shows the estimates of volatility related parameters. BHHH standard errors are in parentheses. The last section of the table shows the log-likelihood values divided by the number of observations T.

A. Yield curve parameters		B. Volatility parameters	
Parameter	Estimate	Parameter	Estimate
$\mathcal{K}^{\mathbb{Q}}_{11}$	-0.022	$M^{\mathbb{Q}}_{11}$	-0.979
	(3.8e-4)		(0.196)
$\mathcal{K}^{\mathbb{Q}}_{22}$	-1.157	$M^{\mathbb{Q}}_{21}$	-1.348
	(0.057)		(0.369)
$\mathcal{K}^{\mathbb{Q}}_{31}$	0.990	$M^{\mathbb{Q}}_{22}$	-1.848
	(0.088)		(0.029)
$\mathcal{K}^{\mathbb{Q}}_{32}$	-6.485	Q_{11}	2.8e-3
	(0.403)		(2.1e-4)
$\mathcal{K}^{\mathbb{Q}}_{33}$	-0.565	Q_{22}	7.6e-3
	(0.023)		(6.8e-4)
γ_0	0.148	k	6.000
	(0.020)		(0.264)
$\lambda^0_{Y,11}$	-1.8e-3	v	-2.120
	(5.5e-4)		(0.121)
$\lambda^0_{Y,21}$	-2.2e-3	σ_f	0.006
	(6.2e-4)		(1.6e-4)
$\lambda^0_{Y,31}$	-0.049	$\Lambda^1_{V,11}$	205.9
	(0.010)		(66.27)
$\lambda^1_{Y,22}$	0.061	$\Lambda^1_{V,12}$	187.1
	(0.114)		(74.71)
$\lambda^1_{Y,31}$	-1.227	$\Lambda^1_{V,22}$	142.3
	(0.077)		(39.40)
$\lambda^1_{Y,32}$	0.491	–	–
	(0.595)	–	–
σ_{MY}	7.65e-7	–	–
	(6.6e-9)	–	–
Loglik y^τ_t/T	38.76	Loglik $v^\tau_{t,RV}/T$	35.85
–	–	Loglik $v^\tau_{t,IV}/T$	4.83

Table V: Model fit

This table gives the in-sample fit for baseline model specification presented in Table IV. Additionally, we report its ability to match the realized and implied volatility dynamics. We report root mean squared error (RMSE) in bps per annum.

	Yields	Realized vol.	Implied vol.
6 month	4.69	–	–
2 year	3.68	25.11	17.87
3 year	3.46	–	–
5 year	4.10	23.21	10.52
7 year	3.17	–	–
10 year	4.50	18.43	9.57

V. Expressions for the volatility of the short rate expectations and term premium

This section provides the formulas for a model-based decomposition of yield volatility into volatility of short rate expectations and term premium volatility. Treasury yield with maturity τ-years can be decomposed as follows:

$$y_t^\tau = \frac{1}{\tau} E_t^{\mathbb{P}} \left(\int_0^\tau r_{t+s} \right) ds + \frac{1}{\tau} \left[E_t^{\mathbb{Q}} \left(\int_0^\tau r_{t+s} \right) ds - E_t^{\mathbb{P}} \left(\int_0^\tau r_{t+s} \right) ds \right]$$
$$- \frac{1}{\tau} \left[\ln E_t^{\mathbb{Q}} \left(e^{-\int_0^\tau r_{t+s} ds} \right) + E_t^{\mathbb{Q}} \left(\int_0^\tau r_{t+s} \right) ds \right],$$

where the first term is the expected average short rate during the life of the bond, the second term is the term premium and the third term is the convexity. We are interested in the conditional volatilities of the first and second term. This requires the computation of the following matrix integrals:

$$S_\tau^{\mathbb{P}} = \int_0^\tau e^{K_Y^{\mathbb{P}} s} ds$$
$$S_\tau^{\mathbb{Q}} = \int_0^\tau e^{K_Y^{\mathbb{Q}} s} ds,$$

where K_Y is the mean reversion matrix of the Y_t process. We compute this integral using the result from Van Loan (1978). Let

$$P = \begin{pmatrix} 0_{3\times 3} & I_{3\times 3} \\ 0_{3\times 3} & K_Y \end{pmatrix},$$

then the integral can be obtained from the upper right block of the following matrix exponential:

$$e^{P\tau} = \begin{pmatrix} I & \int_0^\tau e^{K_Y s} ds \\ 0 & \times \end{pmatrix}.$$

The conditional variance of the term premium of a τ-maturity is given as:

$$Var_t^{rpy,\tau} = \frac{1}{\tau^2} Tr \left[\left(S_\tau^{\mathbb{Q}} - S_\tau^{\mathbb{P}} \right)' \gamma_Y \gamma_Y' \left(S_\tau^{\mathbb{Q}} - S_\tau^{\mathbb{P}} \right) \Sigma(V_t) \Sigma(V_t)' \right].$$

Similarly, the conditional variance of the short rate expectations is:

$$Var_t^{Er,\tau} = \frac{1}{\tau^2} Tr \left[S_\tau^{\mathbb{P}\prime} \gamma_Y \gamma_Y' S_\tau^{\mathbb{Q}} \Sigma(V_t) \Sigma(V_t)' \right].$$

Finally, for each τ-maturity yield, the conditional covariance between the short rate expectations component and the risk premium component can be obtained as:

$$Cov_t^{rpy,Er,\tau} = \frac{1}{\tau^2} Tr \left[S_\tau^{\mathbb{P}\prime} \gamma_Y \gamma_Y' (S_\tau^{\mathbb{Q}} - S_\tau^{\mathbb{P}}) \Sigma(V_t) \Sigma(V_t)' \right].$$

References

Andersen, T. G., and L. Benzoni (2010): "Do Bonds Span Volatility Risk in the US Treasury Market? A Specification Test for Affine Term Structure Models," *Journal of Finance*, 65, 603–655.

Andersen, T. G., and O. Bondarenko (2007): *Volatility as an Asset Class*chap. Construction and Interpretation of Model-Free Implied Volatility, pp. 141–181. Risk Books.

Audrino, F., and F. Corsi (2010): "Realized Correlation Tick-by-Tick," *Computational Statistics & Data Analysis*, 54, 2372–2382, Working paper, Univerisity of St. Gallen.

——— (2012): "Realized Covariance Tick-by-Tick in Presence of Rounded Time Stamps and General Microstructure Effects," *Journal of Financial Econometrics*, 10, 591–616.

Bandi, F., and J. Russell (2008): "Microstructure Noise, Realized Variance, and Optimal Sampling," *Review of Economic Studies*, 75, 339–369.

Britten-Jones, M., and A. Neuberger (2000): "Option Prices, Implied Price Processes, and Stochastic Volatility," *Journal of Finance*, 55, 839–866.

Buraschi, A., A. Cieslak, and F. Trojani (2010): "Correlation Risk and the Term Structure of Interest Rates," Working paper, University of Lugano.

Buraschi, A., P. Porchia, and F. Trojani (2010): "Correlation Risk and Optimal Portfolio Choice," *Journal of Finance*, 65, 393–420.

Carr, P., and L. Wu (2006): "A Tale of Two Indices," *Journal of Derivatives*, pp. 13–29.

da Fonseca, J., M. Grasselli, and C. Tebaldi (2006): "Option Pricing when Correlations Are Stochastic: An Analytical Framework," Working Paper, esliv, University of Padova and University of Verona.

Dai, Q., and K. Singleton (2000): "Specification Analysis of Affine Term Structure Models," *Journal of Finance*, 55, 1943–1978.

Fisher, M., and C. Gilles (1996): "Estimating Exponential-Affine Models of the Term Structure," Working Paper, Federal Reserve Bank of Atlanta.

Fisher, M., D. Nychka, and D. Zervos (1994): "Fitting the Term Structure of Interest Rates with Smoothing Splines," Working paper, Federal Reserve and North Carolina State University.

Fleming, M. J. (1997): "The Round-the-Clock Market for U.S. Treasury Securities," *FRBNY Economic Policy Review*.

Fleming, M. J., and B. Mizrach (2009): "The Microstructure of a U.S. Treasury ECN: The BrokerTec Platform," Working paper, Federal Reserve Bank of New York and Rutgers University.

Gourieroux, C., J. Jasiak, and R. Sufana (2009): "The Wishart Autoregressive Process of Multivariate Stochastic Volatility," *Journal of Econometrics*, 150, 167–181.

Gürkaynak, R. S., B. Sack, and J. H. Wright (2006): "The U.S. Treasury Yield Curve: 1961 to the Present," Working paper, Federal Reserve Board.

Hayashi, T., and N. Yoshida (2005): "On covariance estimation of non-synchronously observed diffusion processes," *Bernoulli*, 11, 359–379.

Hull, J. C. (2005): *Options, Futures and Other Derivatives*. Pretice Hall.

Magnus, J. R., and H. Neudecker (1979): "The Commutation Matrix: Some Properties and Applications," *Annals of Statistics*, 7, 381–394.

Van Loan, C. F. (1978): "Computing Integrals Involving Matrix Exponential," *IEEE Transactions on Automatic Control*, 23, 395–404.

Waggoner, D. F. (1997): "Spline Methods for Extracting Interest Rate Curves from Coupon Bond Prices," *FRB of Atlanta working paper*, 97-10.

Wan, E. A., and R. van der Merwe (2001): *Kalman Filtering and Neural Networks*. John Wiley & Sons, Inc.

Zhang, L., P. A. Mykland, and Y. Ait-Sahalia (2005): "A Tale of Two Time Scales: Determining Integrated Volatility With Noisy High-Frequency Data," *Journal of the American Statistical Association*, 100, 1394–1411.